BOLT BERANEK AND NEWMAN INC

CONSULTING · DEVELOPMENT · RESEARCH

Report No. 1169
Job No. 110862

SOUND PROPAGATION IN RAREFIED GASES

Contract Nonr 3697(00)
Task NR 061-130

Final Report

November 1964

Submitted to:

Office of Naval Research
Code 438
Washington 25, D. C.

Attention:

Mr. Ralph D. Cooper
Head, Fluid Dynamics Branch

SOUND PROPAGATION IN RAREFIED GASES

Contract Nonr 3697(00)
Task NR 061-130

BBN Report No. 1169
BBN Job No. 110862

Final Report

November 1964

Submitted to:

Office of Naval Research
Code 438
Washington 25, D. C.

BOLT BERANEK AND NEWMAN INC.
50 Moulton Street
Cambridge, Massachusetts 02138

SOUND PROPAGATION IN RAREFIED GASES

ABSTRACT

A study of sound propagation in rarefied gases is described with particular emphasis on the propagation in the geometrical relaxation regime where the sound carrying molecules do not suffer intermolecular collisions during the flight from the transmitter to the receiver. The propagation is characterized by the attenuation and the phase parameters. The dependence of these dispersion parameters on the separation between the transducers, the velocity distribution of the molecules subsequent to their interaction with the transmitter surface and the boundary conditions describing molecular-surface interactions is ascertained in terms of a semi-phenomenological theory. Experiments for measuring the dispersion parameters are described and the results are discussed and compared with theory. A theory and an experiment for determining surface accommodation coefficients using sound propagation in rarefied gas are outlined. Finally a theoretical model is constructed that leads to a reasonable qualitative and quantitative description of sound propagation in rarefied gases.

SOUND PROPAGATION IN RAREFIED GASES

TABLE OF CONTENTS CONT.

TABLE OF CONTENTS CONT.

FIGURE CAPTIONS

FIGURE CAPTIONS CONTINUED:

I. INTRODUCTION

The propagation of sound in gases, especially in rarefied gases, offers a method for studying gas dynamics on a molecular basis. From the theoretical point of view this study is particularly attractive since the amplitudes which define the sound field are usually small compared with the amplitudes which define the basic motion of the molecules. Thus, one is able to linearize the kinetic equation of motion. Of particular importance is the linearization of the Boltzmann equation

$$\left(\frac{\partial}{\partial t} + \xi_x \frac{\partial}{\partial x}\right) h(x,\underset{\sim}{\xi},t) = I_{mm}\left\{h(x,\underset{\sim}{\xi},t)\right\} + I_{ms}\left\{h(x=0,\underset{\sim}{\xi},t)\right\} \quad . \qquad (1.1)$$

I_{mm} is the source term arising from intermolecular interactions, I_{ms} is the source term arising from molecular-surface interaction, and $\underset{\sim}{\xi}$ is the molecular velocity vector. The function h represents the perturbation term in the distribution function which is caused by the superposition of the sound field.

A considerable volume of literature[1] exists which deals with methods and techniques for obtaining solutions to the linearized Boltzmann equation. These analyses are confined chiefly to the far field where all memory of surface interaction has been destroyed by intermolecular encounters. One considers a source term in the Boltzmann equation, devoid of any molecular-surface interaction contribution ($I_{ms} = 0$). The results which are obtained indicate that measurements of sound in the far field are sensitive to some of the properties of intermolecular collisions.

The analysis of sound propagation sufficiently near a transmitter surface such that molecules which carry the sound from that surface arrive at the observation point without undergoing intermolecular collisions can also be performed. In this analysis the intermolecular encounters may be ignored ($I_{mm} = 0$). Consequently one expects the solution to the equation of motion to be dominated by molecular-surface interaction parameters. An experimental study of molecular-surface interaction by acoustical means is thus suggested.

In considering the kind of information which one may reasonably expect to obtain from experiments, it is convenient to consider the properties of sound propagation in three distinct regimes of pressure. These are depicted in Fig. 1 and are discussed briefly below.

The first regime may be termed the Classical Regime. Here the emphasis is on quantities which vary little over the mean free path or the mean time of intermolecular collisions. Moreover, molecular-surface effects are quite negligible even at short distances away from the transmitter. Indeed the theoretical expressions which adequately describe sound propagation in the classical regime do not contain detailed kinetic parameters. Nevertheless, the use of the kinetic theory to derive the sound propagation in this regime serves as a limiting criterion for the validity of Eq. (1.1) and may also provide a more fundamental understanding of the nature of sound.

There exists a range of parameters which we designate the Frequency Relaxation Regime. Here the frequency of intermolecular collisions, f_c, is comparable to or smaller than the frequency f of the sound field ($f \gtrsim f_c$), and the sound field is observed at large distances

from the transmitter surface. Then sufficient intermolecular encounters have taken place in the space between the transmitter and the point of observation to ensure that the observed molecules possess no recollection of surface-molecular interactions so that details can be examined entirely on the basis of intermolecular collisions.

In the Geometrical Relaxation Regime the molecules are assumed to traverse the path from the transmitter to the receiver control surface essentially without undergoing any intermolecular collisions. In this case, one sets the source term I_{mm} of Eq. (1.1) zero. The solution of the Boltzmann equation then depends primarily on the molecular-surface interaction. Consequently, an examination of sound propagation in the geometrical relaxation regime could lead to information regarding such interactions.

Our chief concern is with the third regime and the study of molecular-surface interactions. The research reported here is mainly exploratory in nature in both its experimental and theoretical aspects. Nevertheless some of the findings and results contribute in some measure to the understanding of the phenomenon of the propagation of collective ordered motion in a rarefied gas.

II. DESCRIPTION OF THE MODEL FOR DISPERSION STUDIES

To avoid complications in the interpretations of both the experimental and the theoretical results, it is expedient to impose certain constraints on the experimental and theoretical models.

1) The gas molecules only possess translational degrees of freedom and the gas is composed of a "single component."

2) The surfaces of the transmitter and a test surface where the observations of the sound field are carried out (e.g., hypothetical control surfaces or receivers) are plane and parallel to each other.

3) The transmitter surface vibrates uniformly and without distortion.

4) The transmitter is large enough that end effects are negligible.

5) Vibration of a single frequency is superposed on the basic motion of the molecules.

6) The amplitudes which define the sound field are small compared with the amplitudes which define the basic motion of the molecules.

We shall first dwell on the theoretical aspect of the phenomenon.

III. DESCRIPTION OF DISPERSION BY THE ATTENUATION AND PHASE (α AND β)

Consideration of the model defined above permits one to assume a solution to the equation of motion of the form

$$F(x,\underset{\sim}{\xi},t) = F^{o}(\underset{\sim}{\xi}) + h(x,\underset{\sim}{\xi}t) \quad , \tag{3.1}$$

where the function h is small in the mean (i.e. the ratio of a velocity moment in h to one in F^{o} is very much less than unity).

In Eq. (3.1)

x = position of a control surface measured in the direction normal to its plane,

$\underset{\sim}{\xi}$ = molecular velocity vector,

t = time of observation at the control surface,

$F^{o}(\underset{\sim}{\xi})$ = solution to the equation of motion in the absence of sound.

The equation of motion is then the linearized Boltzmann equation which is stated formally in Eq. (1.1).

The sound pressure at the control surface, p(x,t) is the normal flux of alternating momentum at the surface

$$p(x,t) = m \int d\underset{\sim}{\xi}\, h(x,\underset{\sim}{\xi},t)(\underset{\sim}{\xi},\hat{x})^{2} \quad , \tag{3.2}$$

where

m = the mass of each molecule,

$\hat{x}$ = a unit vector in the x-direction.

The dispersive properties of the sound field can be defined by the attenuation per unit distance, α and the wave number β, for waves at angular frequency ω. That there can be a well defined frequency is evident from the separability of Eq. (1.1); and such harmonic disturbances can be induced by imposing an oscillating boundary at the transmitter. The momentum flux (pressure) at any space point thus is of the form $p(x,t) = p(x) \exp(-i\omega t)$. However no assumption has been made that permits one to assume that $p(x)$ is a plane wave and therefore one must obtain the mathematical definition of α and β from an analysis of the measurement process for determining attenuation and phase. One measures the pressure at neighboring space points in the vicinity of x, obtains the difference and normalizes by the interval between the points and the pressure itself. Thus one obtains, for closely neighboring points separated by Δx,

$$\frac{p(x + \Delta x) - p(x)}{\Delta x\ p(x)} = -(\alpha - i\beta) \simeq \frac{\partial p(x)}{p(x)\partial x} \quad . \tag{3.3}$$

Clearly α and β are, in general, functions of x and therefore the sound pressure partial wave of frequency ω at the point x is to be expressed in terms of the sound pressure at x' by the relation

$$p(x) = p(x') \exp - \int_{x'}^{x} ds[\alpha(s) - i\beta(s)] \quad . \tag{3.4}$$

This concept of a generalized attenuation and phase which are not only frequency but also space dependent is fundamental to the subsequent discussion.

Since $p(x,t)$ is a moment over $h(x,\underset{\sim}{\xi},t)$ we must first derive an expression for $h(x,\underset{\sim}{\xi},t)$ in terms of the molecular surface interaction.

IV. DERIVATION OF A GENERAL SOLUTION

A. Formal Solution

Instead of attempting a direct solution of Eq. (1.1) by assuming a suitable form for the source term, we set the source term zero and make that solution subject to the boundary conditions which the source term represents.

We denote the distribution function of the molecules subsequent to their interaction with the vibrating transmitter surface by G_- and the normalized distribution function of the molecules subsequent to their interaction with the transmitter surface in the absence of vibrational motion by g_-. We assume that the incremental velocity, $\underset{\sim}{\sigma}$, and density, $\rho_-^o\eta$, which is imposed on the molecules by the surface vibration are linearly superposed on the molecular motion in the absence of vibrations. The parameter ρ_-^o is the density in the absence of vibrational motion. We denote the distribution function of the incremental velocities by q. G_- is a joint distribution function in $\underset{\sim}{\xi}'$ and $\underset{\sim}{\sigma}$, and can be written in product form because $\underset{\sim}{\xi}'$ and $\underset{\sim}{\sigma}$ are independent. Thus,

$$mG_-(x = 0, \underset{\sim}{\xi}, \underset{\sim}{\sigma}, t') = \rho_-^o\left\{1 + \eta(t')\right\}q(\underset{\sim}{\sigma})g_-(\underset{\sim}{\xi}' - \underset{\sim}{\sigma})U(\xi_x') \quad . \quad (4.1)$$

Here $\underset{\sim}{\xi}'$ = molecular velocity vector,

$$\int d\underset{\sim}{\sigma}\, q(\underset{\sim}{\sigma}) = 1, \quad (4.2)$$

$$\int d\underset{\sim}{\xi} g_-(\underset{\sim}{\xi}) = 1, \quad (4.3)$$

and

$$U(\xi'_x) = \begin{cases} 0 & \xi'_x < 0 \\ 1 & \xi'_x > 0 \end{cases} . \qquad (4.4)$$

We assume that $|\underset{\sim}{\sigma}|/c_m$ and η are small compared with unity and expand g_- in Taylor's series retaining only the first order terms in $\underset{\sim}{\sigma}$

$$g_-(\underset{\sim}{\xi}' - \underset{\sim}{\sigma}) = g_-(\underset{\sim}{\xi}') - \underset{\sim}{\sigma} \cdot \frac{\partial}{\partial \underset{\sim}{\xi}} g_-(\underset{\sim}{\xi}') \quad . \qquad (4.5)$$

Thus, to first order in the perturbation

$$m\underset{\sim}{G}' = m \int \underset{\sim}{G}_- d\underset{\sim}{\sigma} = \rho_-^o \left\{ g_-(\underset{\sim}{\xi}') + \bar{\eta}(t') g_-(\underset{\sim}{\xi}') \right.$$

$$\left. - \bar{\underset{\sim}{\sigma}} \cdot \frac{\partial}{\partial \underset{\sim}{\xi}'} g_-(\underset{\sim}{\xi}') \right\} U(\xi'_x) \quad , \qquad (4.6)$$

where

$$\bar{\underset{\sim}{\sigma}} = \int d\underset{\sim}{\sigma}\, \underset{\sim}{\sigma} q(\underset{\sim}{\sigma}) \text{ and } \bar{\eta} = \int d\underset{\sim}{\sigma}\, \eta\, q(\underset{\sim}{\sigma}) \quad .$$

We introduce a spatial and temporal propagator T to describe the development in time of the distribution function $\underset{\sim}{G}'$ as x goes from zero at the transmitter to its value at the control surface. Formally we denote this development by the equation

$$F(x,\underset{\sim}{\xi},:) = \int dt' \int d\underset{\sim}{\xi}' \; G'(x = 0, \underset{\sim}{\xi}', \underset{\sim}{\bar{\sigma}}, t')$$

$$\cdot \; T(x = 0, \underset{\sim}{\xi}', t' | x, \underset{\sim}{\xi}, t) \quad . \tag{4.7}$$

The determination of the functional form of T is equivalent to solving the Boltzmann equation with corresponding constraints. This usually would present just as many difficulties as the direct solution of Eq. (1.1). However, in the geometrical relaxation regime the propagator assumes the simple form

$$T = \delta(t' - t + \frac{x}{\xi_x}) \; \underset{\sim}{\delta}(\underset{\sim}{\xi}' - \underset{\sim}{\xi}) \quad , \tag{4.8}$$

where δ is Dirac's delta function and $\underset{\sim}{\delta} = \delta_x \delta_y \delta_z$.

From Eqs. (4.6), (4.7) and (4.8) one obtains

$$F = (\rho_-^o/m) \left\{ g_-(\underset{\sim}{\xi}) + \bar{\eta}(t - \frac{x}{\xi_x}) \; g_-(\underset{\sim}{\xi}) \right.$$

$$\left. - \underset{\sim}{\bar{\sigma}}(t - \frac{x}{\xi_x}) \cdot \frac{\partial}{\partial \underset{\sim}{\xi}} g_-(\underset{\sim}{\xi}) \right\} U(\xi_x) \quad ,$$

and

$$h = (\rho_-^o/m) \left\{ \bar{\eta} g_- - \underset{\sim}{\bar{\sigma}} \cdot \frac{\partial}{\partial \underset{\sim}{\xi}} g_- \right\} U(\xi_x) \quad . \tag{4.9}$$

Note that h as given by Eq. (4.9) satisfies the Boltzmann equation with both I_{mm} and I_{ms} equal to zero [see Eq. (1.1)]. The function h satisfies the boundary conditions by virtue of its derivation from Eq. (4.7). To proceed further one must examine these boundary conditions in some detail.

B. Boundary Conditions (Molecular-Surface Interaction at the Transmitter)

Assume that the distribution function of the incident molecules on the surface of the transmitter is $(\rho_+^\circ/m)g_+(\underset{\sim}{\xi})U(-\xi_x)$ [ρ_+° is independent of time in absence of vibrational motion]. Consider the transformation from coordinates fixed in space to coordinates fixed in the vibrating surface of the transmitter. In this coordinate system the distribution function for the incident and emerging molecules is given by $(\rho_+^\circ/m)g_+(\underset{\sim}{\xi} + \underset{\sim}{\mu})U(-\xi_x)$ and $(\rho_-^\circ/m)(1 + \eta)g_-\{\underset{\sim}{\xi} - (\underset{\sim}{c} - \underset{\sim}{\mu})\}U(\xi_x)$ respectively. The velocity $\underset{\sim}{\mu}$ is the velocity of the surface of the transmitter (note that $\underset{\sim}{\mu} = \hat{x}\mu$). Now suppose that the surface does not constitute a source (or a sink) of molecules. One can then equate the incident and reflected fluxes and obtain, after some reduction, the conservation equations

$$\bar{\eta} = a(\mu/c_m) \text{ and } \rho_-^\circ c_- = \rho_+^\circ c_+, \tag{4.10}$$

where

$$a = c_m[(\nu/2c_+) - (\gamma - 1)/2c_-] , \tag{4.11}$$

$$c_{\pm} = \int d\underset{\sim}{\xi}\, \xi_x g_{\pm}\, U(\pm\xi_x) , \tag{4.12}$$

$$\bar{\sigma}_x = \gamma\mu , \tag{4.13}$$

$$\nu\mu = \int_{-\infty}^{t} dt' K(t'|t)\mu(t') , \tag{4.14}$$

$K(t'|t)$ = the probability that a molecule that strikes the surface at time t' emerges at time t.

Here use has been made of the requirement that $g_{\pm}(\underset{\sim}{\xi}) \longrightarrow 0$ as $|\underset{\sim}{\xi}| \longrightarrow \infty$ and we have also made the reasonable assumption that ν and γ are constants in time. Note that ν and γ depend on the type of molecular-surface interaction. The parameter ν is related primarily to the "sitting time" of the molecules on the surface of the transmitter. This surface relaxation time can be sensed by the sound field when the average sitting time is comparable to or longer than the period of the sound oscillation. The parameter γ is related primarily to the efficiency with which the surface impresses its vibrational motion on to the molecules.

The exchange of the normal component of momentum between molecules and surfaces is of great interest to aerodynamicists and may be stated in terms of the ratio, β_T, of reflected to incident normal momentum flux. In the absence of surface vibration this ratio is

$$\beta_T^o = \overline{c_-^2} c_+ / \overline{c_+^2} c_- \quad . \tag{4.15}$$

In terms of properties of the sound field the reflector ratio is

$$\beta_T^a = (\gamma - 1) + (a\overline{c_-^2}/2c_m c_-) \quad , \tag{4.16}$$

where

$$\overline{c_{\pm}^2} = \int d\underset{\sim}{\xi}\ \xi_x^2 g_{\pm} U(\pm\xi_x) \quad , \tag{4.17}$$

and a, $c_{\pm}$ and γ are defined in Eqs. (4.11), (4.12) and (4.13) respectively. Equation (4.16) is a statement that acoustical measurements could be used to ascertain reflective properties of molecular-surface systems.

C. Classification of Surface Interactions

We find it convenient to consider the molecular-surface interaction in terms of three special processes by which the general case may be approximated. Such consideration serves to elucidate the physical interpretation of the quantities ν and γ. These three interaction processes are outlined below:

1. Specular Reflection

Each molecule is assumed to interact with the surface instantly and in such a way that the sign of its component of momentum in the x-direction is reversed. This interaction process conserves energy and momentum. It is easy to show that in this case (viz. Eq. (4.1) et seq.)

$$\gamma = 2 \text{ and } \nu = 1 \quad .$$

2. Diffuse Elastic Reflection

Each molecule is assumed to interact instantly with the surface such that the incident energy is conserved but not the momentum. It is further assumed that the scattering obeys the cosine law of reflection. In this case one can show that

$$\gamma = \frac{3}{2} \text{ and } \nu = 1 \quad .$$

3. Diffuse Inelastic Reflection

The molecules are considered adsorbed by the surface and to come to thermal equilibrium with it before boiling off in a random fashion. That is, it is assumed that neither the momentum nor the energy are conserved, and that the distribution of the

molecules subsequent to the interaction is consistent with the assumption that the gas is in thermal equilibrium with the surface.

In this case there are two regimes. If the function $K(t'|t)$ is such that most of the contribution to the integral in Eq. (4.14) comes from a region where $t - t' < \pi/2\omega$, then $\nu = 1$; in the other extreme $\nu = 0$. For diffuse inelastic reflection $\gamma = 1$.

When more complicated molecular-surface interactions can be approximated by such elementary processes, the contribution from each basic process is computed separately and added to give the total effect.

V. DETERMINATION OF THE TRANSMISSION OF SOUND IN THE GEOMETRICAL RELAXATION REGIME

The equation of sound propagation in the geometrical relaxation regime can be determined using the semi-phenomenological parameters introduced in the previous section. Substituting Eqs. (4.9) and (4.10) in Eq. (3.2) and making straightforward manipulations, we obtain

$$p(s) = \rho_-^o \mu_o c_m^2 \int_o^\infty dr\ r^2 \left\{ a g_-^x(r) - \gamma \frac{\partial g_-^x}{\partial r} \right\} \exp(is/r) \quad , \qquad (5.1)$$

where

$$s = \omega x / c_m \quad , \qquad (5.2)$$

$$r = \xi_x / c_m \quad . \qquad (5.3)$$

Note that Eq. (5.1) is dependent on the molecular-surface interactions in a complex way. There are cases, however, for which it is possible to assume the analytical form of g_+ and g_-; for such cases, ν and γ could be examined by acoustical means. Conversely, if ν and γ could be estimated by an independent method, the distribution function, g_-, could be studied by acoustical means.

Equation (5.1) is suggestive of the work of other investigations. It differs from the equation derived by Meyer and Sessler,[2] but for $s \gg 1$ and for a Maxwellian distribution it yields the same dispersion equations. Our results agree with an equation derived by Kahn[3] when the following restrictions are imposed on Eq. (5.1): the distribution functions are Maxwellian; $\nu = 0$ and $\gamma = 1$ (i.e., diffuse inelastic reflection and $t - t'$ of Eq. (4.14) is, on the average, very much larger than $\pi/2\omega$).

VI. PHYSICAL INTERPRETATION OF SOUND DISPERSION IN THE GEOMETRICAL RELAXATION REGIME

From Eq. (5.1) it is evident that the expression for the sound pressure has the general form

$$p(s) = N \int_0^\infty dr\ A(r)\ \exp\ (is/r) \quad , \tag{6.1}$$

in which N is independent of s. It is through a careful analysis of the significance of the various contributions to the integral in this expression that we uncover the mechanism whereby the sound wave suffers dispersion in propagation.

The integral has an appearance very similar to the Fourier integral and as such can be thought of as being a superposition of weighted plane waves. A(r) would be the weighting function and the phase term exp is/r a plane wave of wave number $\frac{1}{r}$ at dimensionless position s. The weighting function A(r) is the product of the molecular velocity distribution function and a factor which brings the terms N A(r) dr to the dimension of momentum flux, i.e., pressure. Thus the partial sound pressure (the sound pressure contribution from an infinitesimal velocity range) is given by

$$dp(s) = NA(r)\exp(is/r)dr \quad . \tag{6.2}$$

From the above discussion and Eq. (6.2) one can conclude that were there but one velocity there would be no dispersion and the wave number would be inversely proportional to that one velocity.

Extrapolation leads us to state that for a highly peaked flux distribution there would be little attenuation and dispersion. In nature, however, the fluid molecules have a rather broad velocity distribution. For equilibrium and near equilibrium the weighting function A(r) has the general form depicted in Fig. 2a. There is a maximum value of A when r is of the order of unity. Consider now the influence that such a broad weighting function has on a superposition of the partial waves of Eq. (6.2). In the superposition the partial waves can interfere destructively or constructively. The kind of interference contributed in the various ranges of the variable r in the integration can be discussed by considering s/r in the ranges $s/r > 1$ and $s/r < 1$.

The behavior of the phase term as a function of the variables r and s is depicted in Figs. 2b, c and d. For values of s/r large compared with unity the phase term is an oscillatory function of the variable r; the slower molecules ($s > r$) arrive at the receiver with widely varying phases. The partial sound pressures associated with these molecules interfere with one another destructively (phase mixing). Thus the slower molecules do not contribute to the sound pressure. The faster molecules ($s < r$) arrive at the receiver with essentially the same phase. This preservation of coherence by the faster molecules constitutes the sound field at the receiver. The inability of the slower molecules to transmit sound is directly responsible for the dispersive properties of sound. Thus, what constitutes slow or fast molecules is determined by whether the molecules possess velocity components, r smaller or greater than s, respectively. To account for the dispersive properties of sound in more detail it is therefore convenient to consider the problem in three ranges of the parameter s. They are $s \ll 1$, $s \gg 1$ and $s \approx 1$ (see Fig. 2).

In order to introduce some quantitative data in the following discussion reference is made to the example of a Maxwellian distribution. That is, we assume that both g_+ and g_- are Maxwellian distributions. Then from the foregoing equations we obtain

$$N = \rho_o \mu_o c_m \sqrt{\pi}, \tag{6.3}$$

$$A(r) = r^2(a + 2\gamma r) \exp(-r^2) \quad , \tag{6.4}$$

where

$$\mu = \mu_o \exp(-i\omega t),$$

$$\rho_o = \rho_+^o = \rho_-^o$$

and

$$a = \sqrt{\pi}(\nu + 1 - \gamma) \quad .$$

A. Dispersion in the Range $s \ll 1$; Figs. 2a and 2b

In this range only the very slow molecules do not contribute to the sound transmission. Since their associated weighting functions are small they do not impair greatly the total transfer of coherence from the transmitter to the receiver. Thus one would expect the attenuation parameter α to be small and to increase monotonically with increase in s. The phase parameter β (wave number), which is inversely proportional to the speed of sound, is not greatly affected in this range by variation in s. As s increases a corresponding, but slight, decrease in β is expected since it is left to the faster molecules to transmit the sound (coherence).

We cite the results which are computed by solving Eq. (3.4) using Eq. (6.1) and the Maxwellian quantities given in Eqs. (6.3) and (6.4)

$$(\alpha - i\beta)/\beta_o = sa_o[1 + a_1 s^2 + \ldots] - ib_o[1 + b_1 s^2 + \ldots] \quad , \tag{6.5}$$

where

$$a_o = \left(\frac{10}{3}\right)^{1/2} [(a\sqrt{\pi} + 4\gamma)(a\sqrt{\pi} + 2\gamma) - 2(a + \sqrt{\pi\gamma})^2]/(\sqrt{\pi}a + 4\gamma)^2 \quad , \tag{6.6}$$

$$b_o = \left(\frac{10}{3}\right)^{1/2} (a + \sqrt{\pi\gamma})/(\sqrt{\pi}a + 4\gamma) \quad . \tag{6.7}$$

β_o = the phase parameter for an ideal gas under standard condition of temperature and pressure,

$a_1 \ldots b_1$ = constants which depend on ν and γ.

Note that over reasonable limits on ν and γ [$0 < \nu < 1$ and $1 < \gamma < 2$] the value of b_o is near unity.

The quantitative result, Eq. (6.5), bears out the qualitative discussion.

B. Dispersion in the Range s >> 1; Figs. 2a and 2d

In this range only the very fast molecules can participate in transmitting sound. Thus the phase parameter β is small compared with that in the range $s \ll 1$. However, its rate of decrease with increase in s is expected to be proportionately slow. The reason is that the weighting function is a monotonically decreasing function of r; thus the molecules which are concentrated in the vicinity of $r \simeq s$ are those which most influence the transmission. However, the cessation of the oscillation occupies a relatively wide range in the parameter s/r. Both these effects combine to resist large changes in β as a function of s. The attenuation parameter α[N.B. α is a local attenuation variable, see Eq. (3.3)] follows similar changes with s as does the phase parameter, that is, its value decreases at a proportionately slow rate with increase in s.

Again we make use of the Maxwellian distribution to obtain quantitative results for this range. Making use of the method of steepest descent[4] one obtains

$$(\alpha - i\beta)/\beta_o = (\tfrac{5}{24})^{1/2}(\tfrac{s}{2})^{-1/3}\left\{1 - i\sqrt{3}\right\} , \qquad (6.8)$$

which is in agreement with the preceding qualitative discussion. The dispersion in this range is, to first order of approximation, devoid of molecular-surface interaction parameters. The results, Eq. (6.8), are given in graphical form in Fig. 3.

C. Dispersion in the Range s ≃ 1; Figs. 2a and 2c

In the range $r \simeq 1$ the weighting function is relatively large and it undergoes large variation as a function of r. Thus one would expect large variation to occur in both the dispersion parameters.

The attenuation parameter increases as s increases to unity. As s is increased further, the attenuation reaches a maximum value and then decreases to an asymptote for $s \gg 1$. The phase parameter decreases significantly with increase in s only when s becomes greater than unity. For only then is the weighted mean velocity component of the faster molecules in the direction of propagation increased.

In this range we were not able to obtain analytical expressions for p(s) or its derivative with respect to s, therefore, we performed numerical computations. The results are plotted in Fig. 3. Observe that the dependence of the dispersion on the molecular-surface interaction parameters is present but not pronounced. This is unfortunate; it indicates that considerable accuracy in the measurements of the dispersion of sound is required to obtain results that can distinguish between the various processes of surface-molecular interactions.

VII. EXPERIMENTAL WORKING RANGE

In order to extend the range of the work which has been previously conducted in this field,[2,5,6] as well as to examine new applications where sound propagation may be useful for studies of rarefied gas dynamics, we chose to conduct our experiments at lower frequencies* (2 to 12 kc) and at lower pressures* (as low as 5×10^{-5} mm Hg). The lower frequency range has the advantage that sound measurements can be made in a truly rarefied gas over larger separations. Measurements over longer distances have the advantages that higher accuracies can be achieved and that auxiliary equipment can be chosen without the pains of miniaturization. The challenge to this approach is whether one can produce high enough signals and sensitive enough receivers to achieve measurements with low signal-to-noise at the lower pressures.

---

* Greenspan[5] conducted his measurements at 11 Mc and at relatively high pressures, higher than 1 mm Hg. Meyer and Sessler[2] conducted their experiments at 100 and 200 kc and at pressures in excess of 2×10^{-3} mm Hg.

VIII. THE EXPERIMENTAL SYSTEM FOR STUDIES OF DISPERSION

In this section, we describe briefly the experimental system which we used to study the dispersion of sound in rarefied air. The system is designed to operate in pressure ranges where the mean free path of intermolecular collisions is longer than the spacing between the transmitter and receiver.

A. The Vacuum System

For good accuracy and flexibility, it is desirable that the spacing between the transmitter and receiver be varied over several centimeters. Separations of the order of 1 cm or more require working pressures of the order of 10^{-3} mm Hg or lower. (In air the mean free path at 10^{-3} mm Hg and 300° K is about 5.5 cm.) Since mechanical pumps cannot achieve these low pressures, it is necessary to use a diffusion pump.

The pumping system, which is of conventional design, is shown in Fig. 4. The limiting pressure obtained in the test section with this system was about 3×10^{-5} mm Hg.

The transmitter-receiver and the bell jar-base plate systems are shown in Fig. 5. The sound source (transmitter) is mounted on a movable vacuum tight rod which can be actuated externally. With this arrangement, the distance between the source and receiving microphone can be varied continuously over a range of 12 cm while maintaining a constant pressure in the test section.

Two vacuum gauges are incorporated in the system. A thermocouple gauge is used in the range from 10 mm Hg to 5×10^{-3} mm Hg and an ionization gauge covers the range from 5×10^{-3} mm Hg to 10^{-6} mm Hg. We also had available an alphatron gauge with a range from 10 mm Hg to 10^{-3} mm Hg.

B. The Electrical and Mechanical System

The microphone is of the electrostatic type (Bruel and Kjaer Model 4132). A 1-inch microphone is suspended vertically above the sound source in a fixed location. It is mounted in such a way that the electrical connections are through the top of the bell jar. This arrangement is chosen in order to reduce the background signals due to electrical stray currents. The polarization voltage of the microphone is set so that no discharge occurs between membrane and backing plate at the operating pressure.

The sound source is an electrostatic transducer with solid dielectric. The vibrating diaphragm is light enough so that mechanical cross talk between it and the microphone is essentially eliminated. The vibrating surface extends to about a 5.0 inch diameter. The output of the sound source has a maximum of 130 db at atmospheric pressure.

The electrical diagram of the experimental apparatus is shown in Fig. 6.

The separation between microphone and transmitter can be varied automatically, continuously and slowly over a range of about 12 cm. The initial separation may be set as small as 0.05 cm. The separation x as a function of time is given by

$$x = b + d[1 - \cos(t/\tau)] \quad , \tag{8.1}$$

where b is the initial separation (which can be varied independently), d = 12.1 cm and τ is set at about 90 seconds (τ may also be controlled independently). This particular rate of change of stroke was decided upon because it is simple to implement and also enables one to

expand the initial region ($t \ll \tau$) where the attenuation and phase parameters show definite deviation from the theory in which multiple reflections are neglected. The disadvantage of this variation is that the records have to be converted to a linear scale. We have therefore installed mechanical and electrical linear scale converters which can be "switched in" when records over large separations are desired. With these converters operating, the abscissa of the graphic record is proportional to the distance travelled by the transmitter. With these devices, it is estimated that the spacing can be read to better than 0.1 cm over the entire range of separation.

The sound pressure level is recorded on a graphic level recorder and can be read to within 0.5 db on a 50 db potentiometer. When a limited range of the sound pressure level is of interest a 10 db potentiometer is used and the accuracy thereby improved. The results which are reported here were obtained with a 50 db potentiometer only. Typical records are reproduced in Fig. 7. The identation in Fig. 7a at about 1 cm is due to an approximately 10 db change in gain which is sometimes necessary to keep the entire record on a 50 db potentiometer.

The phase is measured with a phasometer which indicates the phase difference between a direct signal from the driving oscillator and the signal received at the microphone. The output of the phasometer is fed into the ordinate of a graphic recorder. We estimate that in most cases the phase could be read to within 10° over a phase change of 360°. A typical record is shown in Fig. 8. The jumps in the curves (at 2 cm and around 10 cm) occur when one full meter scale reading (360°) is completed.

The useful frequency range of the present apparatus extends from 5 kc to about 12 kc. The upper limit is set by the sensitivity of the microphone which drops off considerably beyond its resonance at about 10 kc. The lower limit is set by the available stroke of 12 cm. Lower frequencies are useful for studies of multiple reflections only.

IX. EXPERIMENTAL RESULTS

All of the many records which were taken (e.g., Figs. 7, 8, and 9) show that there are two distinct regimes in the behavior of the amplitude and phase of the transmitted sound. There is the "initial region" (up to approximately 1 cm) where the signal decreases very rapidly and the sign of the phase is opposite to that predicted by the theory. It is only at a separation of more than 1 cm that the attenuation and the phase of the signal follow, at least qualitatively, the theory outlined above.

The region, where multiple reflections can be ruled out ($x \gg 1$ cm), we term the "far field." The region between these two extremes we refer to as the "intermediate region." Roughly, the initial region, the intermediate region and the far field correspond to regions which are defined by $s \ll 1$, $s \sim 1$ and $s \gg 1$ respectively, where s is the normalized separation. We shall now consider each region separately.

A. The Initial Region

We found that the initial decay with increasing separation is independent of the pressure down to 5×10^{-5} mm Hg for a given frequency, and up to a separation of about 1 cm. A slight variation of the initial decay with variation in frequency is observed. We conclude that for small separations (< 1 cm) and at a given frequency the decay with distance is independent of the pressure (this was observed over pressures ranging from 5×10^{-5} mm Hg to 10 mm Hg) in the frequency range from 2 to 8 kc. To establish that the initial decay is not a result of a possible variation in amplitude and phase over the surface of the transmitter, the phenomenon was examined at various sections of the transmitter. The results of these experiments show no variation in the detailed

structure of the initial decay curve. Furthermore, we replaced the electrostatic transmitter by a 5-inch plane piston radiator (first resonance at about 15 kc) which was driven by an electromechanical shaker. We compared the initial decay curves obtained at various pressures and found them to be the same within the accuracy of the measurements. The piston radiator was only used in the lower frequency range (< 3 kc) due to its poor efficiency at higher frequencies.

Using our theory, we are able to partially account for the behavior of the sound in this region. That the slope of the sound pressure level curve is independent of pressure at small separations may be explained when one considers that for small separations, the attenuation and phase in the geometrical relaxation regime resemble the corresponding parameters in the classical regime. This resemblance is not only qualitative but also quantitative (see Section VI). Since the attenuation and phase define the transmission of sound and since we see no reason why the presence of multiple reflections should alter this correspondence, no transition region is to be expected as one proceeds from the classical regime to the geometrical relaxation regime.

B. The Intermediate Region

In this region, commencing first at higher frequencies (c.f. Fig. 9), the multiple reflections fade and the response is predominately the response of a single reflection at each surface. Figures 7 and 9 (which are representative figures) show that the attenuation is relatively small in this region. However, it increases somewhat with increasing separation. Comparison with Fig. 3 indicates that this behavior is in agreement with theory. The phase also assumes a behavior which is more commensurate with the single reflection theory.

C. The Far Field Region

In this region, ($x > 2$ cm) we can test the theory which we derived above. The experimental results are plotted in Figs. 10 and 11. As abscissa in these figures, we use the quantity $R = (2/3\pi)(f_c/f)$[6] It is related to the gas pressure p_o through f_c, the mean frequency of intermolecular collisions. A corresponding parameter can be defined for the geometrical relaxation regime, $R_x = 2/3\pi\ c_m/(xf) = 4/(3s)$. Then c_m/x is the mean frequency of molecular-surface collisions. Note that in the geometrical relaxation regime the attenuation and phase are independent of the collision frequency f_c and hence of the ambient pressure.

Curves predicted by the classical Burnett theory and the values predicted by our theory (in the geometrical relaxation regime) are also plotted. The computations are based on the diffuse elastic process of molecular-surface interaction. There is an excellent agreement between theory and experiment in the geometrical relaxation regime. The experimental data which are analyzed for values of the dimensionless separation parameter $s = 5.22$ and $s = 10.44$ seem to favor the diffuse elastic process of molecular-surface interactions (see Fig. 3). However, more refined experiments and analyses of the data would be required before a definite conclusion on the type of surface interaction is justified.

The transition between the frequency relaxation regime and the geometrical relaxation regime is of special interest. If one accepted the Burnett theory as fairly representative of the situation in the classical, and in the frequency relaxation regime (even in the range of pressures where $\Lambda\omega/c_m < 2$) then one might conclude (from Figs. 10 and 11) that the transition region from the frequency relaxation regime to the geometrical relaxation

regime extends over a pressure range of about half a decade. This is particularly evident in Fig. 10 where this transition region extends into the range of pressure for which the attenuation has its maximum value. The experimental data here have values which fall somewhere between the Burnett predictions and those from the theory which applies to the geometrical relaxation regime (c.f. Fig. 3).

The predictions of the present theory are based on the assumption that the velocity distribution of the molecules subsequent to their interaction with the surface is Maxwellian. We have not ascertained the magnitude of the deviation from this distribution that is required to significantly influence the results, however there is consistency between this assumption and the experimental data.

X. SOUND PROPAGATION IN RAREFIED GASES -- WAVE CONCEPT

In this section a wave theory approach to the interpretation of sound propagation in rarefied gas is briefly expanded. The purpose of this analysis is to construct an alternative analysis to the one of the particle concept that was given above. This is brought out not only to reassess the results obtained by the particle concept but also in the hope that some aspects of the problem that cannot easily be interpreted in terms of the one may be more readily interpreted by the other. In particular, the phase reversal that occurs in the initial region is explained more readily by the wave concept.

A. The General Idea

First consider only those molecules that have the same thermal speed $c = (\xi_x^2 + \xi_y^2 + \xi_z^2)^{1/2}$ * and assume specular reflection. Then the speeds before and after interaction with the vibrating surface are equal (except for the small ac component), and the molecules leaving a surface element are equally distributed over all angles. The molecules which emerge from a surface element have properties which are the same as that of a wave emanating from a surface element. They have a given speed of propagation and they are equally distributed over all angles. Therefore, the additional average momentum that is given to the molecules by a vibrating surface element can be considered as a wave propagating out from this surface element.** Thus by treating

---

* We impose an isotropic velocity distribution.

** This is not the usual particle-wave analogy where the particle itself is represented by a wave whose wavelength is given by the total momentum of the particle. In our case, only the additional momentum represents a wave.

the molecules carrying coherent momentum from the surface by the technique of wave propagation analysis one makes use of the elements of classical acoustics to interpret sound propagation in a rarefied atmosphere. There is also the convenience that the angular distribution is averaged out initially.

B. Radiation from a Moving Surface

Still considering only molecules with the same thermal speed c take the velocity of the moving surface element dS to be u and define a wave number $k = \omega/c$ (ω = angular frequency of the driver). The elemental sound pressure dp that is generated by the surface element dS at a distance h is then[7]

$$dp = -i\rho u\omega \frac{\exp(ikh)}{2\pi h} dS \quad . \tag{10.1}$$

(ρ = density of the gas.)

The result for the total vibrating surface S is obtained by integrating over dS. To obtain the actual sound pressure in a rarefied gas all values of c must be considered. This is accomplished by multiplying Eq. (10.1) by the distribution function F(c) for the thermal speed c and integrating over dc. Thus

$$p = -u\rho \int_0^\infty \int_S \frac{\omega \exp(ikh)}{2\pi h} F(c)\, dc\, dS \quad . \tag{10.2}$$

For a gas at equilibrium

$$F(c) = \frac{4}{\sqrt{\pi}} \frac{c^2}{c_m^3} \exp[-(c/c_m)^2] \quad . \tag{10.3}$$

Therefore

$$p = \frac{4}{\sqrt{\pi}} u \int_o^\infty \frac{c^2}{c_m^3} \exp[-(c/c_m)^2]$$

$$\cdot \left\{ \int_S \frac{-i\omega\rho \exp(ikh)}{2\pi h} dS \right\} dc \quad . \qquad (10.4)$$

Thus for any configuration for which the radiation behavior (the integral over S) is known the propagation properties can be found by integrating over the speeds of propagation. This is especially useful if one wishes to calculate the sound propagation from a complicated transmitter system in a rarefied gas. To apply Eq. (10.4) one calculates the wave propagation from the geometry, multiplies it by the velocity distribution function and integrates over all possible values of c.

C. Radiation from an Infinite Disk

For radiation from an infinite disk the integration over S is readily performed. The integral in the brackets yields the expected plane wave. One obtains

$$-\int_{S \to \infty} \frac{i\omega\rho \exp ikh}{2\pi h} dS = \rho c \exp ikx = \rho c \exp(i\omega x/c) \qquad (10.5)$$

in which x denotes the normal distances from infinite disk to receiver.

By inserting Eq. (10.5) into Eq. (10.4) one obtains for the pressure

$$p = \frac{4}{\sqrt{\pi}} u\rho c_m \int_0^\infty r^3 \exp[-r^2 + i(s/r)]\, dr \quad , \qquad (10.6)$$

where

$$r = c/c_m \quad \text{and} \quad s = \omega x/c_m \quad .$$

This is exactly Eq. (5.1) for specular reflection. ($\nu = 1$, $\gamma = 2$.)

Since ρ and c_m are known, a measurement of u together with a known solution of the integral (i.e., for $s > 3$) provides a method of checking numerical constants in Eq. (10.6). Such a measurement, if its accuracy is better than 1 db, would indicate whether specular or diffuse reflection is dominant. This accuracy could be attained only by refinement of the above experimental design.

D. Nonspecular Reflection from the Transmitter

The above calculations included only the case of specular reflection. Other reflection properties could also be considered by using the "wave concept." However, to do this one would have to know the radiation properties of materials with finite impedance (how much sound is radiated from a vibrating and absorbing surface?). Unfortunately, no complete solution of this problem is available. We assume that impedance of a moving disk alters mainly the amplitude of the radiated sound; other effects seem to be less important. (This seems to hold for diffuse elastic and diffuse inelastic reflections.) Thus, we continue to confine the discussion to specular reflection only in using the wave concept.

E. A Finite Microphone in Front of an Infinite Transmitter (Sound Waves under Standard Conditions)

Consider the transmitter-microphone system depicted in Fig. 12. The classical sound pressure p_s as measured by the microphone can be expressed by

$$p_s = u\rho c_c \frac{(1 + R) \exp ikx}{1 - R^2 \exp 2ikx} \quad . \tag{10.7}$$

(u = velocity of the transmitter, k = wave number, R = reflection coefficient.)

Equation (10.7) is obtained by adding up all the reflected waves. Note that for $R \ll 1$, one obtains the usual plane wave solution. R is a complicated function of x, d and $\lambda = \frac{2\pi}{k}$, the wave length. For the subsequent discussion we need only know its limiting behavior. For $x \ll d$, $R \approx 1$; and for $x \gg d$, $R \longrightarrow 0$. As x varies from $x \ll d$ to $x \gg d$, one would expect a monotonic transition between these two limiting values of R.

Consider the phase changes that occur when x is increased. For $kx \ll 1$ and $R \approx 1$ we have approximately

$$p_s = u\rho c_o/-ikx \quad .$$

Thus, the phase shift between u and p_s is $\pi/2$. For $R \approx 0$ we have

$$p_s = u\rho c \exp ikx \quad .$$

The phase shift is kx. If the transition from $R \approx 1$ to $R \approx 0$ occurs before $kx = \pi/2$, there must be a minimum in the phase shift as shown in Fig. 13. This phase transition is indeed observed (see Fig. 8). Note that the point where $R \approx 0$ is reached depends primarily on the microphone size.

F. A Finite Microphone in Front of an Infinite Transmitter in a Rarefied Gas

One obtains the sound propagation by multiplying Eq. (10.7) by F(c) and integrating over c. This gives

$$p(s) = up \frac{4}{\sqrt{\pi}} \int_o^\infty \frac{c^3}{c_m^3} \exp[-(c/c_m)^2] \cdot \frac{(1 + R) \exp(i\omega x/c)}{1 - R^2 \exp(2i\omega x/c)} \, dc \quad . \tag{10.8}$$

For $R \approx 1$ and $\omega x \ll c_m$ we can approximate this

$$p(s) = up \frac{4}{\sqrt{\pi}} \int_o^\infty \frac{c^4}{-ic_m^3 \omega x} \exp[-(c/c_m)^2] \, dc \quad , \tag{10.9}$$

or

$$p(s) = \frac{3}{2} \frac{up c_m^2}{-i\omega x} = \frac{9}{5} \frac{up c_o}{-ikx} \quad . \tag{10.10}$$

Equation (10.10) differs from the corresponding sound wave solution only by a factor 9/5.

G. An Attempt to Explain the Measured Results

Calculated curves for limiting cases are presented in Fig. 14. In order to normalize the data, the square of the sound pressure at each separation is divided by $u^2\rho^2c_m^2$. As before, $s = \omega x/c_m$.

The decay from s = 1 to s = 8 is calculated from

$$|p(s)|^2 \approx |p(s = 1)|^2 \exp\left\{-2 \frac{\alpha}{\beta_o} \beta_o \Delta x\right\}$$

$$= |p(s = 1)|^2 \exp\left\{-0.4 \sqrt{6/5}\ (s - 1)\right\} \qquad (10.12)$$

by using the value $\alpha/\beta_o \approx 0.2$ (c.f. Fig. 3). The plot of the result of this calculation is labeled Eq. (10.12) in Fig. 14. For the decay in the region $s \ll 1$ we take R = 1 and use Eq. (10.10). This calculation is represented by the portion of the curve labeled Eq. (10.10). Between the calculated curves Eq. (10.12) and Eq. (10.10) extrapolated transitions can be constructed. The transition curves depend on the transition from R = 1 to R = 0. The two extreme cases of transition are depicted in Fig. 14, that of a fast transition from R = 1 to R = 0 and that of slow transition between these limits.

Figure 15 shows a comparison between the estimated and measured values. The measured values were taken from Fig. 9. The results favor a fast transition from R = 1 at $s \ll 1$ to R = 0 for $s > 1$.

The pressures at x = 0.05 cm are adjusted to be equal. Therefore, u/ω must be the same in both cases. This implies that in the 10 kc case the amplitude of the transmitter is five times as high as that of the 2 kc case. Thus, one would expect the 10 kc curve to

be approximately 14 db higher than the 2 kc curve for $s > 1$, i.e., when the initial decay region has been passed. The difference between the two curves at $x = 3$ cm is 10 db. We add to that 5 db. This represents the excess attenuation of the 10 kc wave over the 2 kc wave in reaching the point $x = 3$ ($s = 5.1$). Then the data agree.

XI. REFLECTION OF SOUND FROM SOLID SURFACES

The results of experiments for both the amplitude and phase, expecially at small separations, suggest the possibility of observing reflection of sound from solid surfaces at low pressures. Also recall that the experimental results favor the conclusion that interaction of molecules with solid surfaces is predominantly diffuse elastic. This is in agreement with the finding of Stickney[8] who used a molecular beam and a Rayleigh disc to measure the momentum transfer between a gas and metallic surface.

We set up an experiment to examine the reflection of sound directly, as shown in schematic form in Fig. 16. With this arrangement there is no direct path between the transmitter and receiver. The sound reaches the microphone primarily by reflection from the test surface. The results obtained are shown in Fig. 17. The records illustrate clearly that reflection of sound can be measured in a rarefied gas. Moreover, the results in Fig. 17 show that standing wave patterns of a sort occur also at low pressures. The maxima and minima of the standing waves may be used, as they are used at higher pressures, to determine reflection properties (e.g., relative accommodation coefficients) of surfaces at reduced pressures.

If one assumes that the distance between two minima is directly proportional to c/ω, c being the phase velocity of propagation, then the results in Fig. 17 imply that the phase velocity of sound increases with a decrease in pressure. This is in agreement with the phase variation with pressure reported in Figs. 10 and 11.

More refined techniques would be required to make the measurements useful. However the results obtained thus far do give encouragement that such an approach may be successful.

XII. VARIATION OF SOUND PRESSURE LEVEL AS A FUNCTION OF PRESSURE

The results obtained for the variation of sound pressure level as a function of separation (e.g., see Fig. 7) indicate that the decay at small separation is independent of the pressure (in the range of multiple reflections). To examine this phenomenon in a more direct way, we measured the variation of the sound pressure level as a function of pressure at a frequency of 6 kc and a constant separation of 0.35 cm ($s \approx 0.32$).

The result of this experiment is shown in Fig. 18. A curve based on a linear relationship is also plotted. The range of pressure covered by this experiment extends from 6 mm Hg down to 1.4×10^{-4} mm Hg. The pressures were measured by an ionization gauge from 1.4×10^{-4} mm Hg to about 5×10^{-3} mm Hg and with an alphatron gauge in the range from 7×10^{-3} mm Hg to 6 mm Hg. Note that slight discrepancies between theory and experiment occur at the limit of the gauge range (for the ionization gauge the upper limit is at 5×10^{-3} mm Hg) or where a switch of scale takes place (the alphatron scale has to be switched at intervals of a factor of ten in pressure starting at 10^{-2} mm Hg). These are the positions where one may expect inaccuracies in the gauges to be most pronounced. The break in the curve at about 10^{-2} mm Hg also shows that the calibration of the two gauges differs by a small amount. The transition region from the classical to the geometrical relaxation regime occurs in the range of pressure of about 1.5×10^{-2} mm Hg. Since the curve does not exhibit a changing slope, our argument that no change would be expected in the range where s is much smaller than unity is substantiated.

XIII. EXPERIMENTS FOR THE MEASUREMENT OF SURFACE ACCOMMODATION COEFFICIENTS

A. Outline of the Theory

A configuration useful for the study of surface reflections is given in Fig. 19. S_1 is the surface under study. S_2 is a control surface used to define a source of coherent momentum fluctuations and S_3 is a control surface used to define the coherent part of the distribution function of those molecules reflected from S_1.

As in the previous development, we ignore the source terms in Eq. (1.1) and subject the homogeneous equation to boundary conditions appropriate to the configuration under study. Then the relationship between the distribution function at phase point $\underset{\sim}{r}_n, \underset{\sim}{\xi}_n$ at time t_n to the distribution functions at the phase point $\underset{\sim}{r}_m \underset{\sim}{\xi}_m$ at t_m in a region having no collisions may be described by a propagator $T_{nm}(\underset{\sim}{r}_n \underset{\sim}{\xi}_n t_n | \underset{\sim}{r}_m \underset{\sim}{\xi}_m t_m)$ as in Eq. (4.7). n denotes the transmitting control surface and m the receiving control surface. However, when studying surface interactions, one must give explicit consideration to the transformation caused by the surface itself. By denoting the distribution function of those molecules striking surface S_1 by F_{-S_1} and those leaving by F_{+S_1}, one can indicate the surface transformation symbolically by

$$F_{+S_1} = M_{S_1}(F_{-S_1}) \quad . \tag{13.1}$$

It is to the determination of M_{S_1} that we direct our efforts in this section.

The control surface S_2 is essentially a source of "test" molecules, i.e. molecules having a coherent momentum fluctuation characterized by the fluctuating velocity $\underset{\sim}{\sigma}$. The control surface S_3 is established to assess the distribution function and/or velocity moments of those molecules arriving from S_1 which have retained this coherent momentum. Thus it is necessary to express F_{-S_3}, the distribution of molecules arriving at S_3 in terms of F_{+S_2} via the propagators T and the surface transformation M_{S_1} . This relationship is expressed as follows:

$$F_{-S_3}(\underset{\sim}{r}_3, \underset{\sim}{\xi}_3, \underset{\sim}{\sigma}, t_3) = \int \cdots \int \{d\tau\}\, T_{13} M_{S_1} T_{21} F_{+S_2} \cdot (\underset{\sim}{r}_2, \underset{\sim}{\xi}_2, \underset{\sim}{\sigma}, t_2) \quad . \tag{13.2}$$

$\{d\tau\}$ represents the elemental variables of all initial and intermediate phase points on the appropriate surfaces. As in Eq. (3.1) F_{-S_3} can be separated into a dominant incoherent part F^o and a coherent perturbation h. Thus,

$$F_{-S_3} = F^o_{-S_3} + h(\underset{\sim}{r}_3, \underset{\sim}{\xi}_3, \underset{\sim}{\sigma}, t_3) \quad . \tag{13.3}$$

We first determine whether measurements of h or of moments over h can determine parameters which can be used to characterize M, the surface interaction operator.

It is convenient to express the operator M as a sum of three terms

$$M = M_s + M_{de} + M_{di} \quad . \tag{13.4}$$

Each term is related to one of the three processes of surface interaction as discussed in Section IV.C. Expressing M in this manner amounts to the assumption that the three processes, specular, diffuse elastic, and diffuse inelastic reflections, are linearly independent. Such an assumption may be valid provided one seeks to describe only the gross properties of the molecular-surface interactions. M_s, M_{de} and M_{di} are the operators describing the processes of specular, diffuse elastic and diffuse inelastic interactions respectively.

Equation (13.4) can be substituted in Eq. (13.2) to yield a decomposition of h, Eq. (13.3), into three parts:

$$h = h_s + h_{de} + h_{di} \quad . \tag{13.5}$$

The receiver is in general a momentum sensitive device and is capable therefore only of measuring a linear combination of moments of the distribution function. The suitability of an experiment to determine surface interaction parameters is dependent on the manner in which the properties of M_{S_1} influence the velocity moments at S_3. The result is a function of θ_{21} and θ_{13} as evidenced by the expression Eq. (13.2). Consider as a representative moment, the momentum flux calculated from Eq. (13.5). Since each of the contributing components of h is a different function of angle, the total momentum can be written

$$p_{S_3} = R_s \Omega_s(\theta_{21}, \theta_{13}) + R_{de} \Omega_{de}(\theta_{21}, \theta_{13}) \quad . \tag{13.6}$$

R_s and R_{de} are the measures of the specular and diffuse elastic reflection and are related to the momentum accommodation coefficient of the two processes. Ω_s and Ω_{de} are in general complex functions

of the sizes of surfaces S_2 and S_1. The term involving the diffuse inelastic reflection is missing in Eq. (13.6) since this process destroys the coherent fluctuating momentum of the impinging molecules.

Equation (13.6) is of exceptional complexity. It is therefore necessary to introduce constraints related to specific experiments so designed that their interpretation can be related to a simplified form of Eq. (13.6). Such simplification can be obtained if the surfaces S_2, S_1 and S_3 can be made small enough so that the path of propagation from S_2 to S_3 can be specified to a good approximation by θ_{21} and θ_{13} only. A schematic representation of the experimental system is shown in Fig. 20a. For such a system, Eq. (13.6) can be approximated

$$p_{S_3} \propto [R_s \Omega_s^2(\theta_{21},\theta_{13}) + R_{de}\cos(\theta_{13})] \quad . \tag{13.7}$$

Here $\Omega_s^o(\theta_{21},\theta_{13})$ is a function such that it is equal to unit when $\theta_{21} = \theta_{13}$ and approaches zero rapidly as $|\theta_{21} - \theta_{13}|$ increases. An approximate expression for this function can be formally written

$$\Omega_s^o(\theta_{21},\theta_{13}) = \left[\frac{\sin(\theta_{21} - \theta_{13})}{\theta_{21} - \theta_{13}}\right]^{2n} \quad , \tag{13.8}$$

where n is a positive integer. θ_{21} and θ_{13} in Eq. (13.8) are expressed in radians. In Eq. (13.7) we assume that diffraction effects from the edges of surface S_1 are negligible.

By keeping both the distances and the source output constant, measurements of p_{S_3} as a function of the angle θ_{13} should lead to determination of such ratios as

$$\frac{p_{S_3}(\theta_{13} = \theta_{12})}{p_{S_3}(\theta_{13} \neq \theta_{12})} = \frac{R_s}{R_{de}} + \frac{\cos(\theta_{12})}{\cos(\theta_{13})} \quad , \tag{13.9}$$

from which the ratio R_s/R_{de} can be ascertained. If a baffled opening is used to replace the reflector surface, an arrangement that is illustrated in Fig. 20b, the measured sound pressure at S_3' is proportional to

$$p'_{S_3}(\theta'_{13} = \theta_{12}) \propto R_s + R_{de} + R_{di} = 1 \quad . \tag{13.10}$$

When the source strength and distances involved are maintained equal in both experiments, an additional ratio can be obtained, namely

$$\frac{p_{S_3}(\theta_{13} \neq \theta_{12})}{p'_{S_3}(\theta'_{13} = \theta_{12})} = R_{de}\cos(\theta_{13}) \quad . \tag{13.11}$$

Hence, one should obtain the relative mangitudes of R_s, R_{de} and R_{di}. The baffled hole experiment can serve further as a check that diffraction effects are indeed negligible. This is achieved by measuring $p'_{S_3}(\theta'_{13} \neq \theta_{12})$ and ensuring that $p'_{S_3}(\theta'_{13} \neq \theta_{12}) \ll p'_{S_3}(\theta'_{13} = \theta_{12})$.

B. Outline of the Experiment

The schematic arrangement given in Fig. 20 shows the experimental setup: S_2 represents a 1.25-inch transmitter, S_1 represents a 1-inch circular aluminum disk, S_1' represents a 1-inch hole in the center of a 5-inch aluminum baffle and S_3 represents a 1-inch microphone. The distances ℓ_{21} and ℓ_{13} are each 3-inches. S_3 is attached to a 3-inch long arm (ℓ_{13}) that can be actuated externally when the system is in the bell jar. The arm can be actuated to move the microphone in a circular path in a plane containing the centers of S_2, S_1 (or S_1') and S_3 (or S_3') with S_1 as the center point. The geometrical relationship between the various components are thus not fine enough to make Eqs. (13.7) and (13.10) applicable in an absolute sense, nevertheless we hoped that a rough approximation could be achieved. However, the signal-to-noise ratio was too low and no dependable results are reported.

To improve the signal-to-noise a more powerful transmitter was designed and constructed. With the more powerful transmitter, the signal-to-noise ratio is still too low. It appears that at least 10 to 20 db higher signals are required in order to obtain meaningful results. This is not possible with our existing tools. We believe there is yet the possibility of carrying out such an experiment successfully. Two suggestions follow:

1. Replace the source at S_2 by a reasonably collimated and powerful molecular beam and place a transmitter at S_1. Equation (13.6) should then be modified to accommodate the new arrangement. Such a modification can be derived using the methods of Section IV.B.

2. Replace the source at S_2 by a collimated and powerful molecular beam that is chopped at a fixed frequency. By the time the fluctuating disturbance reaches the surface S_1, the large amplitudes would have diminished sufficiently to be considered small and the molecules will have predominantly a fluctuating component of momentum at the frequency of the chopper. Both the collimation and the higher amplitudes that can be obtained at S_1 by this means should contribute more than 20 db to the signal to noise ratio making the experiment feasible.

XIV. A KINETIC THEORY MODEL OF SOUND PROPAGATION

There is a close quantitative correspondence between the results of Section VI which we obtained for the geometrical relaxation regime and those which are obtained in the classical and frequency relaxation regimes.[1] The point of departure is that in the latter regimes one must identify the variable s with the mean free path, $s = \omega\Lambda/c_m$, whereas in the geometrical relaxation regime it is defined in terms of the normal distance from the transmitter to the point of observation, Eq. (5.2). However, in both cases these lengths represent the free flight path between collisions. Since the dispersive properties of sound in the geometrical relaxation regime are related to the free flight path, we infer from this correspondence that dispersion in the other regimes can be related to the free flight. We propose the following model. In the classical and frequency relaxation regimes a coherent ensemble of molecules travels an average distance of one mean free path without collision. In a collision process a new ensemble of molecules is statistically established to which the coherence is communicated. This ensemble of molecules now becomes the carrier of this portion of the sound field. Between collisions, the motion is essentially in the geometrical relaxation regime and is subjected to the loss of coherence typical of that regime. In a subsequent collision process the residual coherence is once more established in an ensemble of molecules which has a basically similar molecular distribution to the preceding ensembles; and so on. Thus, with the proper interpretation as to what constitutes sound propagation in the classical and the frequency relaxation regimes, a simple model can be constructed to account for the dispersive properties of sound in these regimes.

A simple way of constructing the model is to envision collision control surfaces as depicted in Fig. 21. We characterize the collision process and the subsequent emergence of a fluctuating component of velocity by a function of velocity $\phi(v_x)$. At the zeroth control surface the fluctuating component in the density pertaining to those molecules that travel in the positive x-direction is given by

$$\rho_o = \int_o^\infty \phi(v_x)\, F(v_x)\, dv_x \quad , \tag{14.1}$$

where $F(v_x)$ is the distribution function of molecular velocities in the positive x-direction. In travelling one mean free path from the zeroth to the first control surface, the corresponding density fluctuation at the first control surface is given by

$$\rho_1 = \int_o^\infty \phi(v_x)\, F(v_x) \exp(i\lambda\omega/v_x)\, dv_x \quad . \tag{14.2}$$

Proceeding in this manner, it can be readily shown that the density fluctuation at the Nth surface is given by

$$\rho_N = \rho_o[\rho_1/\rho_o]^N \quad . \tag{14.3}$$

The fluctuating component in the distribution function leaving the Nth surface is given by

$$h_N = [\rho_1/\rho_o]^N\, \phi(v_x)\, F(v_x) \quad . \tag{14.4}$$

Denote the distance from the initial control surface where the sound is generated to a control surface where the sound is finally measured by x. Then

$$x = N\Lambda + \delta x \quad , \tag{14.5}$$

where $\delta x/\Lambda < 1$. Since the sound measuring device is a momentum flux (pressure) assessor, the relationship between the sound pressure at $x = 0$, p_o, and $x = N + \delta x$, $p(x)$, is given by

$$p(x) = p_o[\rho_1/\rho_o]^N \left(\frac{1}{\rho_o}\right) \int_o^\infty \phi(v_x)\, v_x^2\, F(v_x) \cdot \exp(i\delta x\omega/v_x)\, dv_x \quad . \tag{14.6}$$

If N is large, Eq. (14.6) can be readily approximated by

$$p(x) \approx p_o[\rho_1/\rho_o]^{(x/\Lambda)} \quad . \tag{14.7}$$

Thus in the frequency relaxation regime the pressure and the density fluctuations obey essentially the same dispersive laws. This is of course in sharp contrast to the geometrical relaxation regime where the density fluctuations and the pressure fluctuations do not necessarily obey the same dispersive laws.

If, in an experiment, the planes perpendicular to the direction of propagation where observations of the sound pressure are made are separated such that N_{21} is large,

$$N_{21} = \frac{x_2 - x_1}{\Lambda} \gg 1 \quad , \tag{14.8}$$

where x_1 is the location defining the first plane and x_2 the second plane, then the attenuation and phase parameters are given by

$$\alpha - i\beta = -\frac{1}{\Lambda} \ell n(\rho_1/\rho_o) \quad . \tag{14.9}$$

Alternately if $N_{21} < 1$, the attenuation and phase parameters are similar to those of the geometrical relaxation regime, namely,

$$\alpha - i\beta = -\frac{i\omega}{c_m} \frac{\int_o^\infty \phi(v_x) v_x F(v_x) \exp(i\Delta x\omega/v_x)\, dv_x}{\int_o^\infty \phi(v_x) v_x^2 F(v_x) \exp(i\Delta x\omega/v_x)\, dv_x} \quad , \tag{14.10}$$

where $\Delta x = x_2 - x_1$. Observe that the attenuation and phase parameters in Eq. (14.10) are independent of the ambient pressure.

For the transition region from $N_{21} \gg 1$ to $N_{21} < 1$ the dispersion properties can be derived from Eq. (14.6); however, the expressions in this case are more complex.

To calculate further one must explicitly know the function $\phi(v_x)$. This function embodies the collision processes of molecular-molecular interactions. In Section VI we showed that the dispersive properties are not very sensitive to the details of the dependence of the interactions on the velocity v_x, and consequently one would expect Eq. (14.9) to yield results that are not very sensitive to the explicit dependence of $\phi(v_x)$ on v_x. This proves to be true. For any finite polynomial function

$\phi(v_x)$, Eq. (14.9) yields attenuation and phase parameters that show similar behavior to that of the corresponding geometrical relaxation parameters depicted in Fig. 3, with Λ in place of x. The experimental results support this conclusion, as is apparent from the data of Figs. 3, 10 and 11.

Although there are theories which lead to dispersion laws for normal gases and plasmas, it remains a point of continued discussion to obtain a physical description of the dispersive properties uncovered by these formal theories. The procedure that we have suggested above has the advantage that the physical interpretation is present in the model. We emphasize the essential distinction between a model of this type which is motivated by its physical content and other models that have been used in this type of problem which are motivated more by their solvability. The conceptual basis is simply that the dispersive properties of sound in gases is directly determined from an assessment of the average amount of "free flight" that the molecules experience.

REFERENCES

1. Review of contemporary works and many references may be found in H. Grad, "Theory of Rarefied Gases," and F. S. Sherman and L. Talbot, "Experiment Versus Kinetic Theory of Rarefied Gases," in Rarefied Gas Dynamics (F. M. Devienne Ed.), Pergamon Press, London, 1960.

2. E. Meyer and G. Sessler, z.f. Phys. 149, 15, 1957.

3. D. Kahn, "Kinetic Theory of Sound Propagation in Rarefied Gases," Ph.D. Thesis, Yale University, 1962.

4. P. M. Morse and H. Feshbach, Method of Theoretical Physics, McGraw-Hill Book Company, Inc., 1953, Chapter 4.

5. M. Greenspan, J. Acoust. Soc. Am. 28, 644, 1956.

6. F. S. Sherman and L. Talbot, "Experiment Versus Kinetic Theory of Rarefied Gases," Rarefied Gas Dynamics, Proceedings of the First International Symposium held at Nice, edited by F. M. Devienne, Pergamon Press, 1960.

7. P. M. Morse, Vibration and Sound, McGraw-Hill Book Company, Inc., Second Ed., 1948, p. 327.

8. R. E. Stickney, Phys. Fluids 5, 1617, 1962.

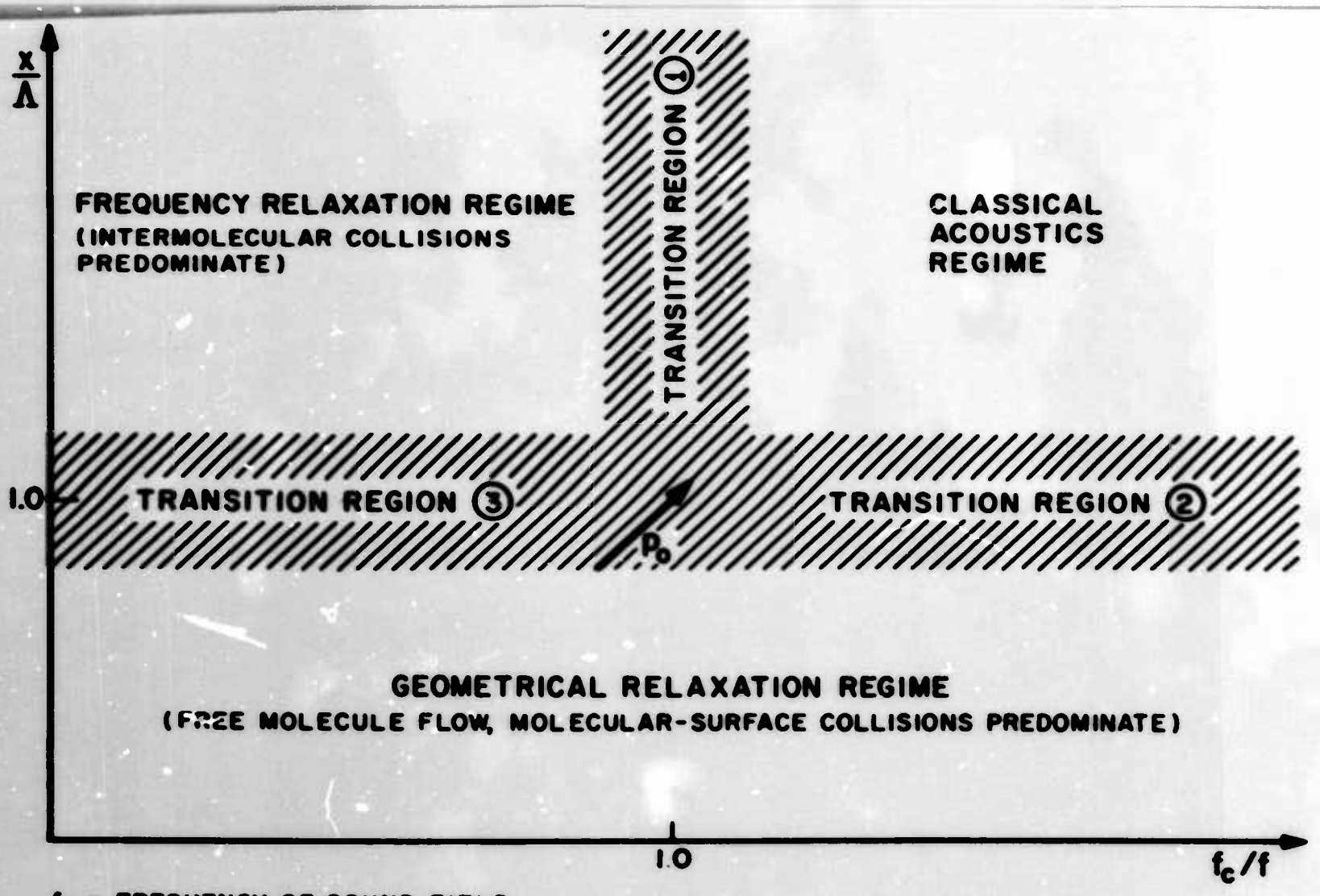

f = FREQUENCY OF SOUND FIELD
f_c = MEAN FREQUENCY OF INTERMOLECULAR COLLISIONS
Λ = MEAN FREE PATH OF INTERMOLECULAR COLLISIONS
x = DISTANCE FROM TRANSMITTER TO OBSERVATION POINT
c_m = MOST PROBABLE THERMAL SPEED OF MOLECULES
p_o = PRESSURE OF THE GAS

FIG. 1 THE 3 REGIMES OF SOUND PROPAGATION

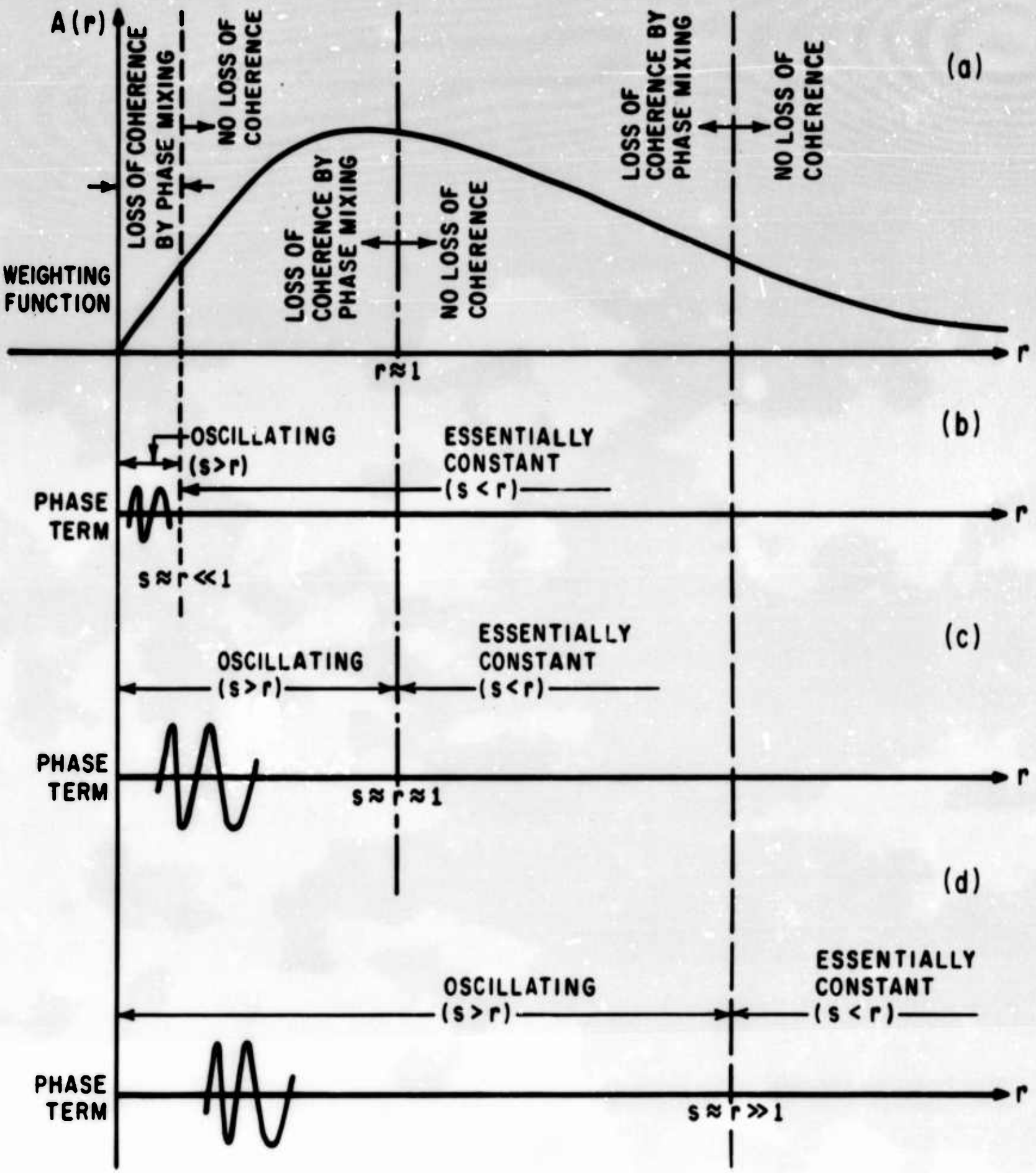

FIG. 2 RANGES OF DESTRUCTIVE AND CONSTRUCTIVE INTERFERENCE FOR THE 3 RANGES OF s

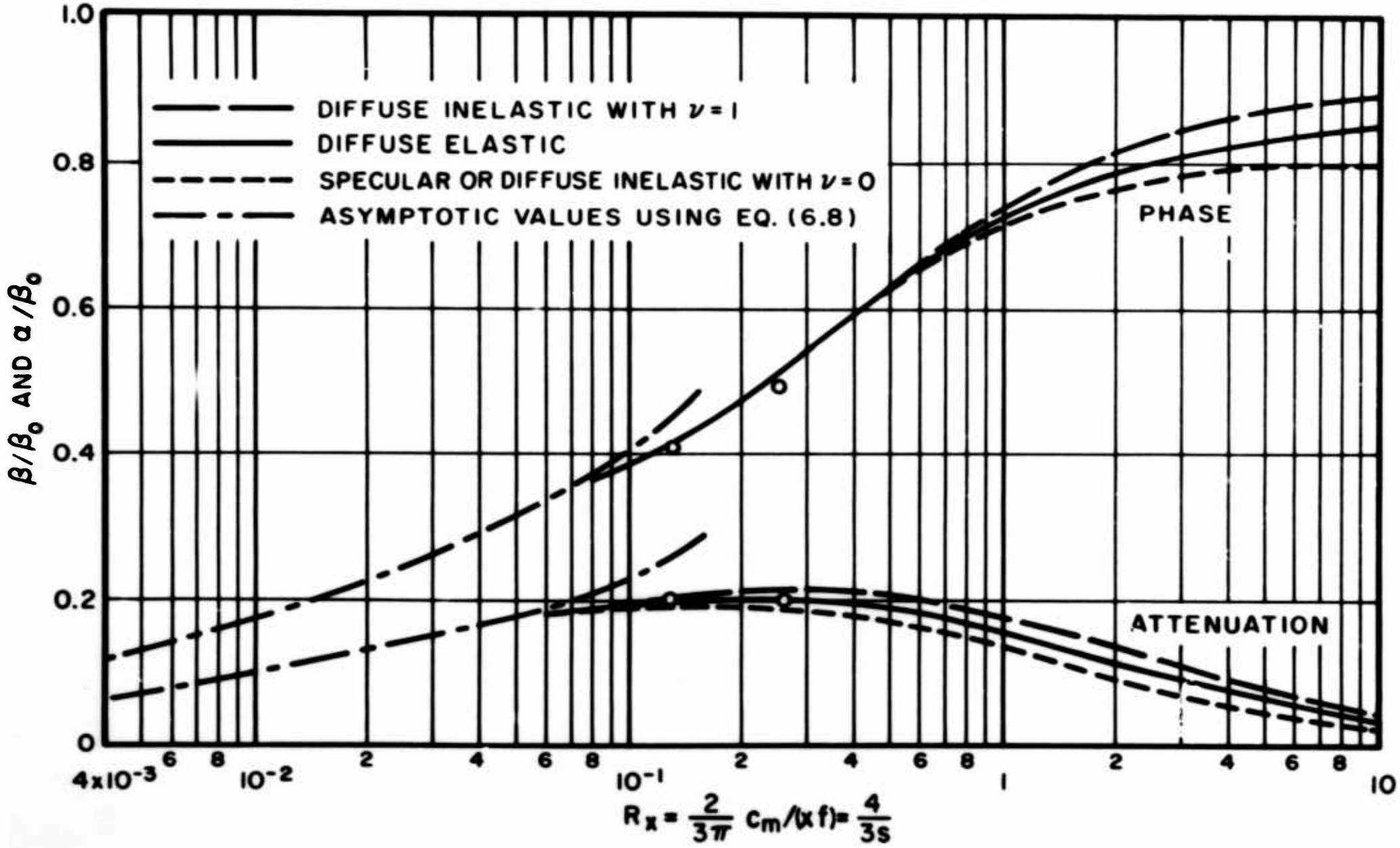

FIG. 3 COMPUTED ATTENUATION AND PHASE FOR SEVERAL TYPES OF SURFACE INTERACTIONS (o EXPERIMENTAL VALUES, SEE FIGS. 10 AND 11)

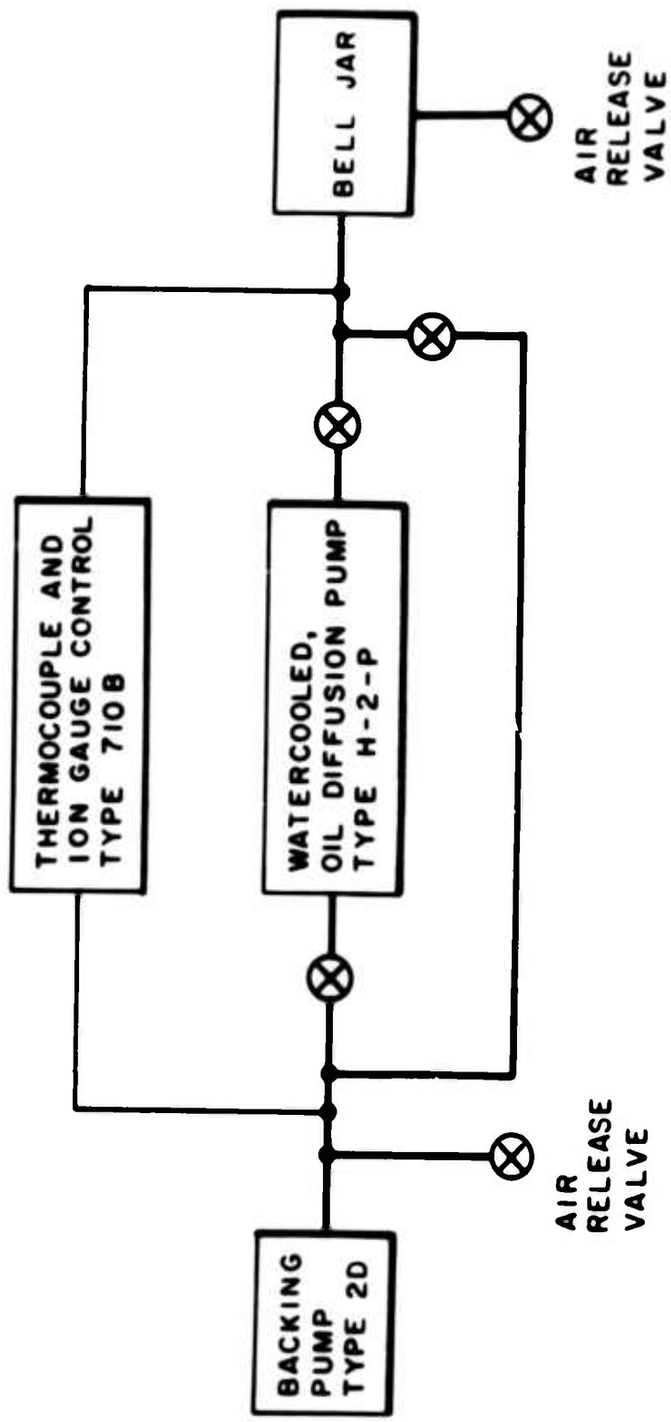

FIG. 4 SCHEMATIC SKETCH OF THE PUMPING SYSTEM

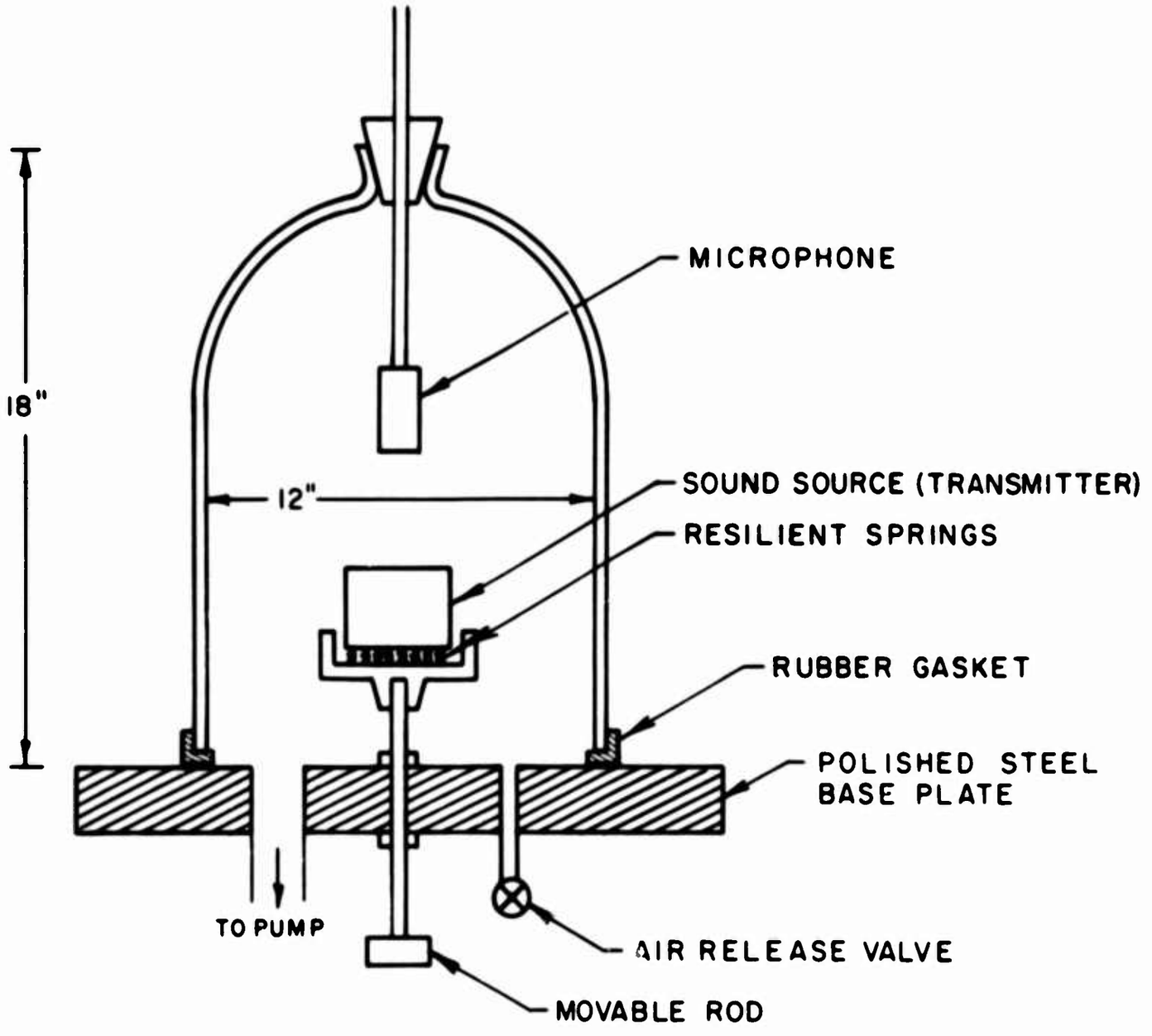

FIG. 5 SKETCH OF THE TRANSMITTER-MICROPHONE SYSTEM

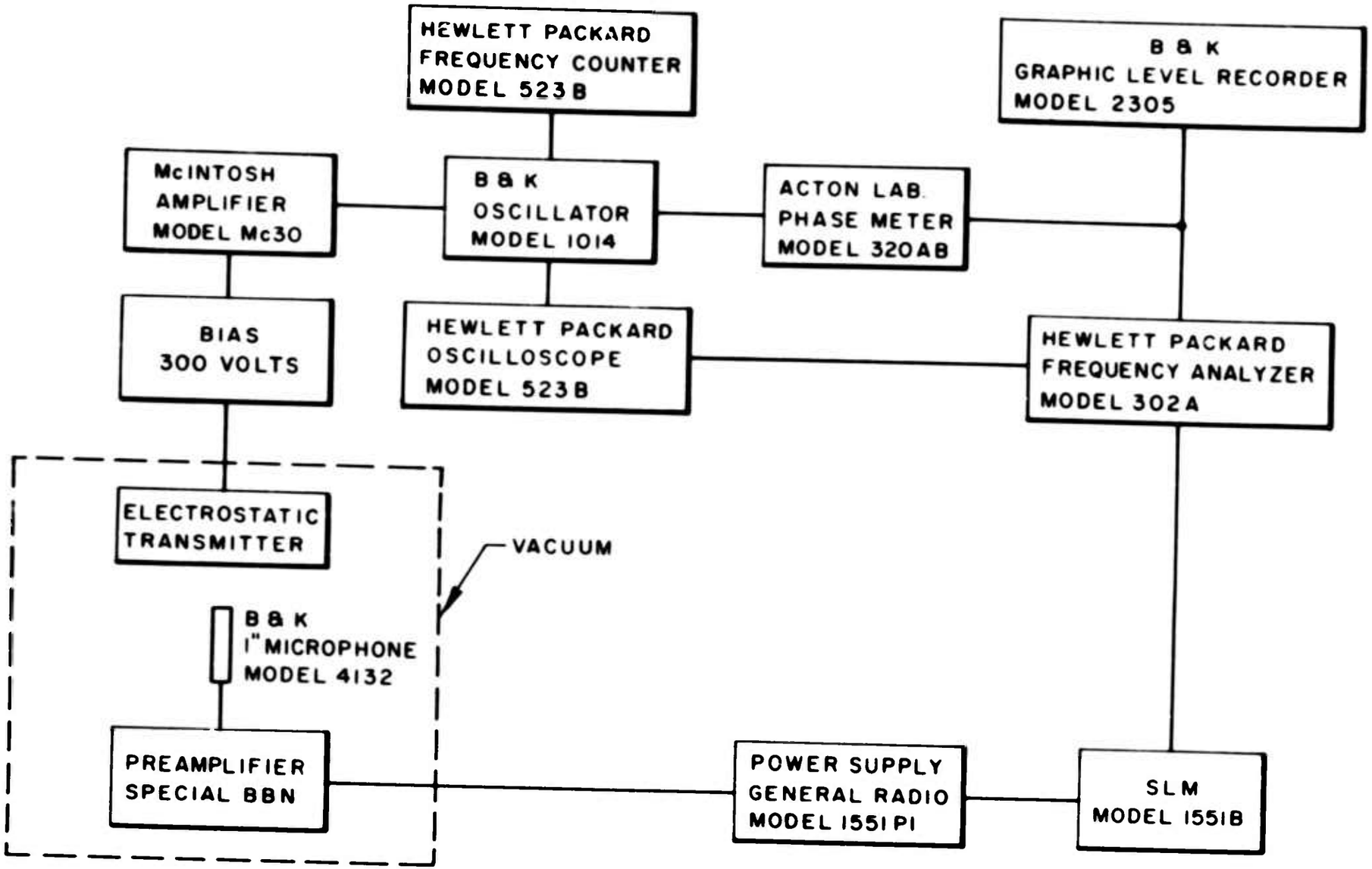

FIG. 6 ELECTRICAL FLOW DIAGRAM

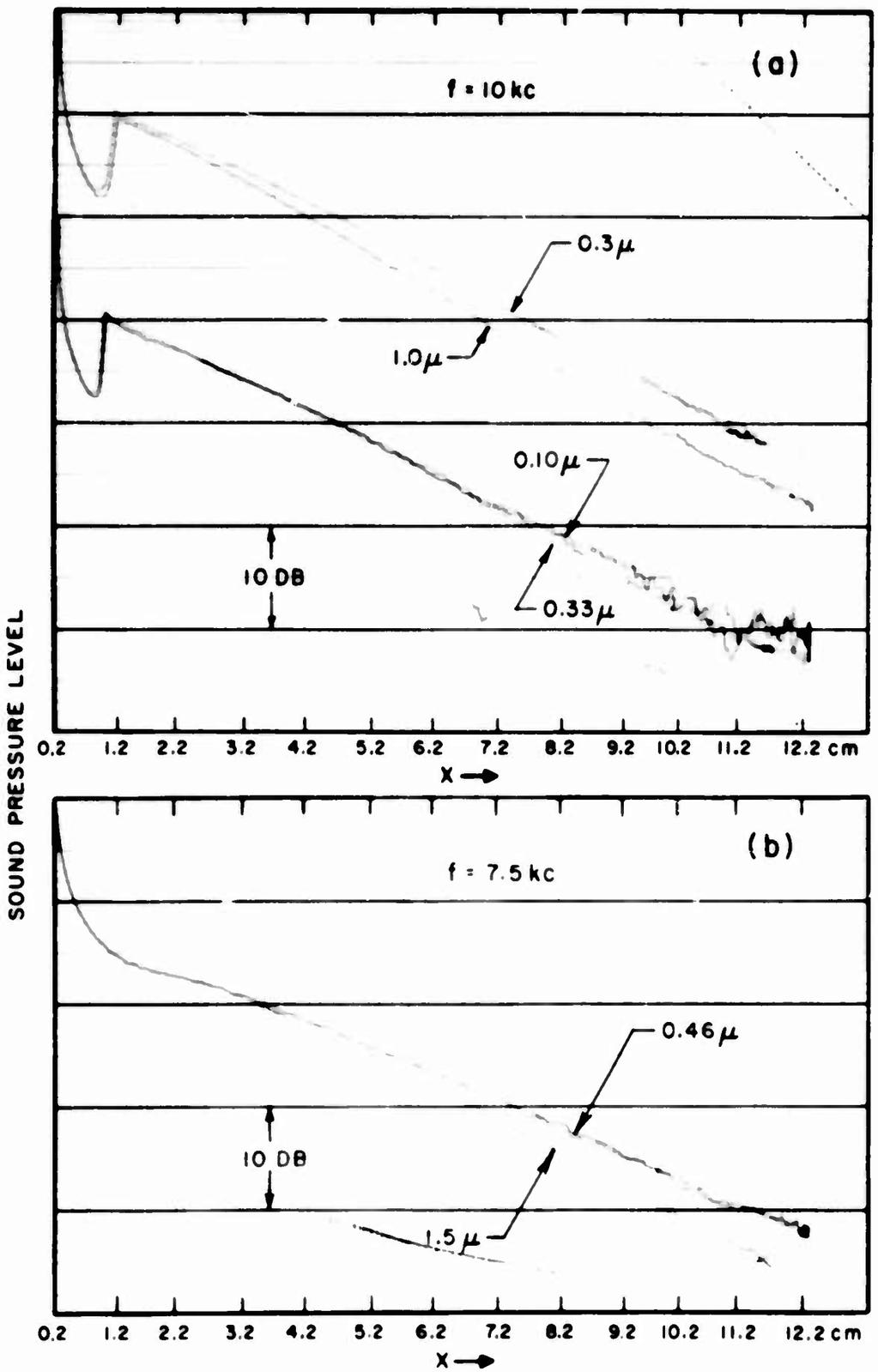

FIG. 7 TYPICAL RECORDS OF SOUND PRESSURE LEVEL VS. SEPARATION

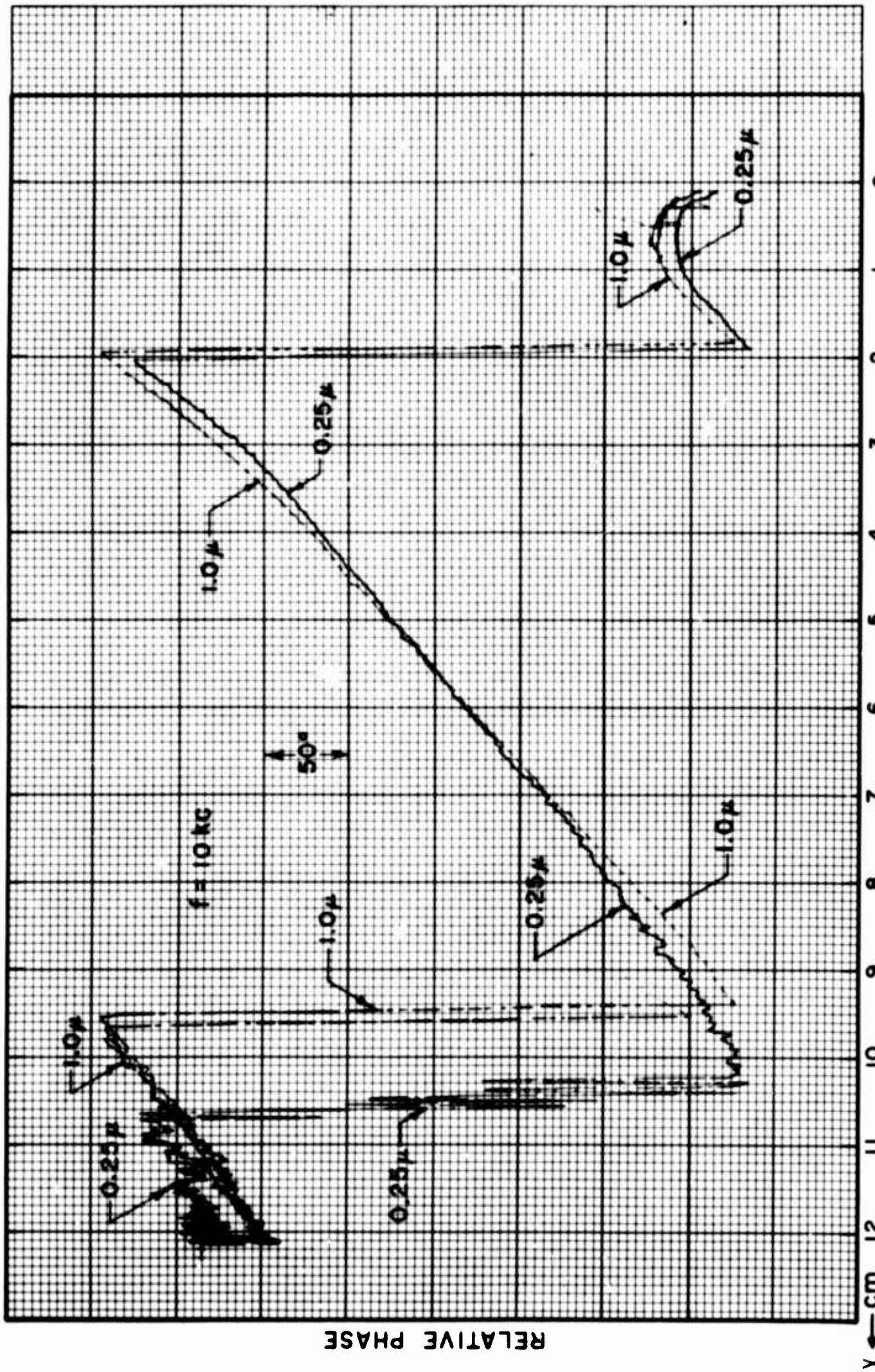

FIG. 8 TYPICAL RECORDS OF PHASE VS. SEPARATION

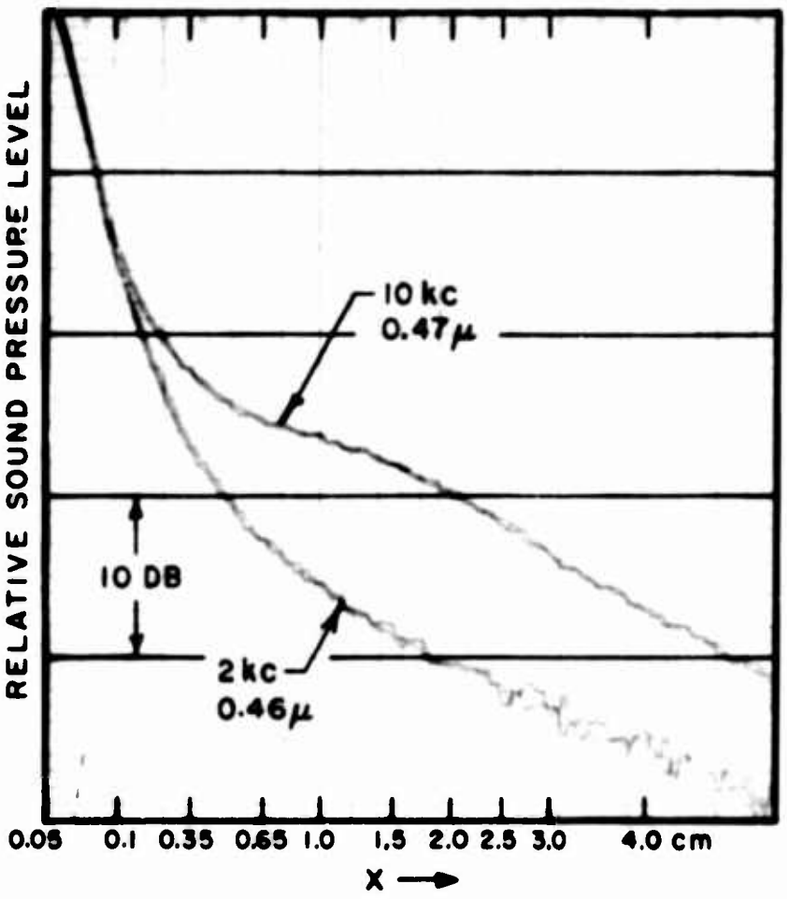

FIG. 9 INITIAL DECAY CURVES FOR DIFFERENT FREQUENCIES (10 kc AND 2 kc) AT PRESSURES OF 0.46 μ

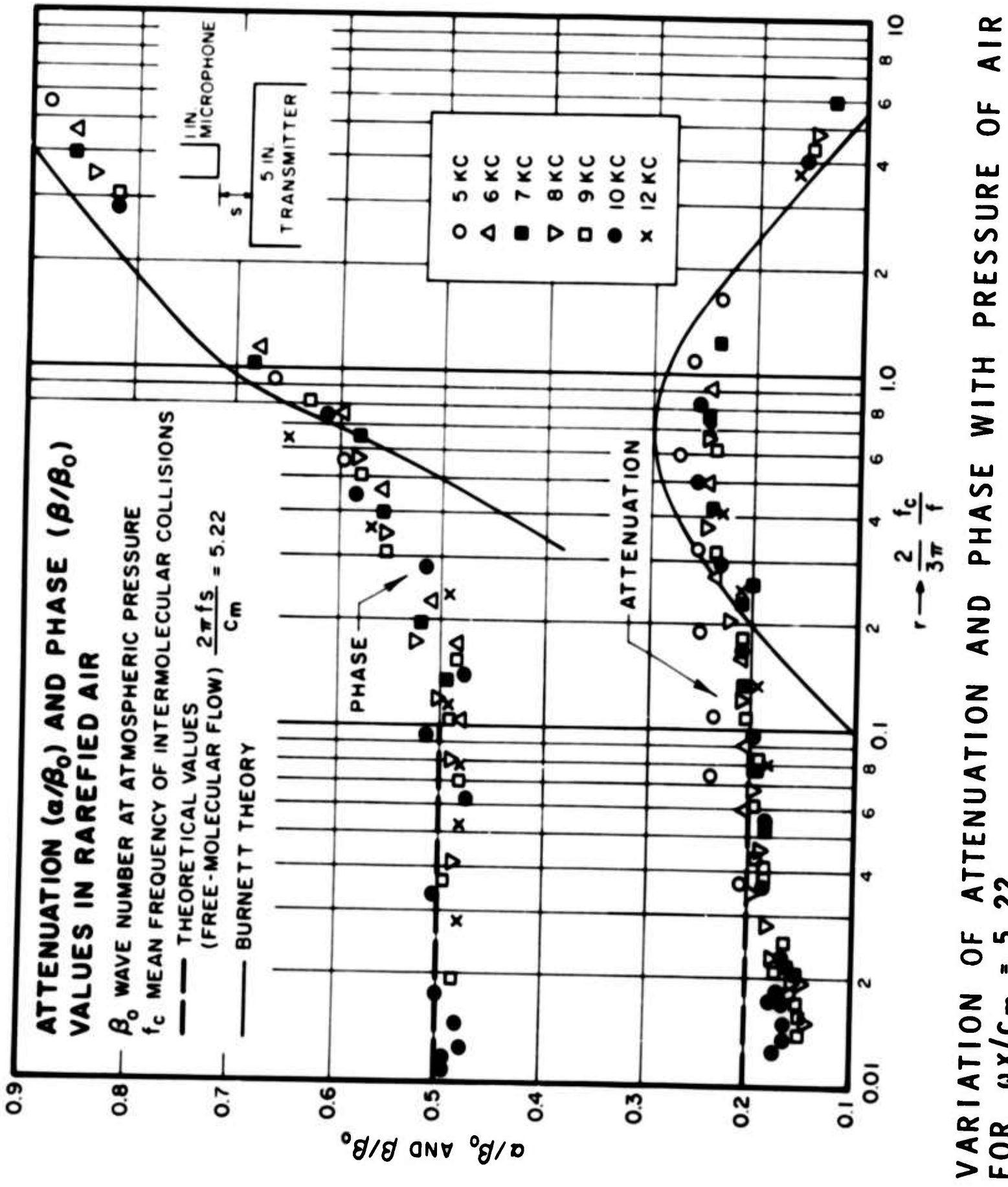

FIG. 10 VARIATION OF ATTENUATION AND PHASE WITH PRESSURE OF AIR FOR $\omega x/c_m$ = 5.22

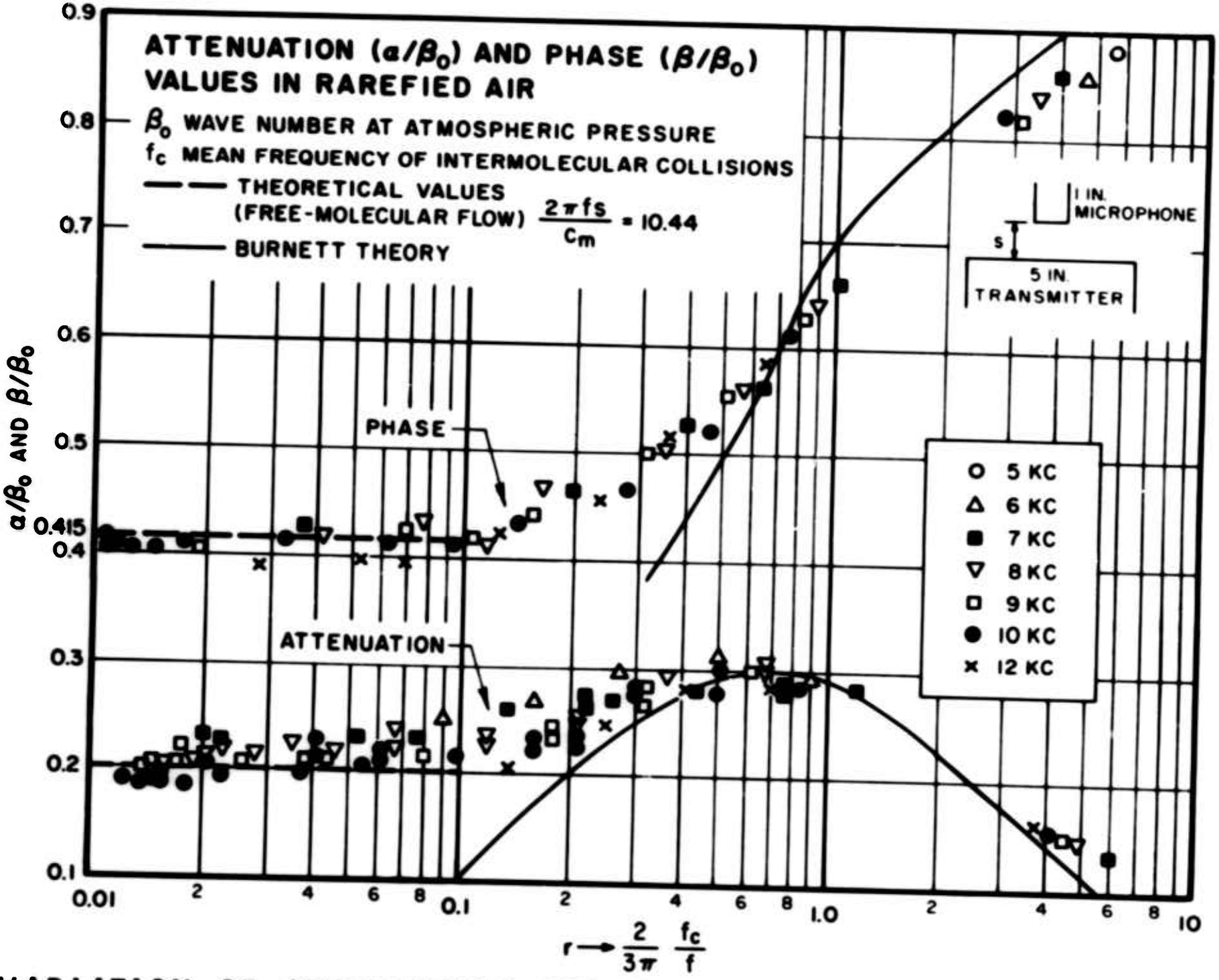

FIG. 11 VARIATION OF ATTENUATION AND PHASE WITH PRESSURE OF AIR FOR $\omega x/c_m = 10.44$

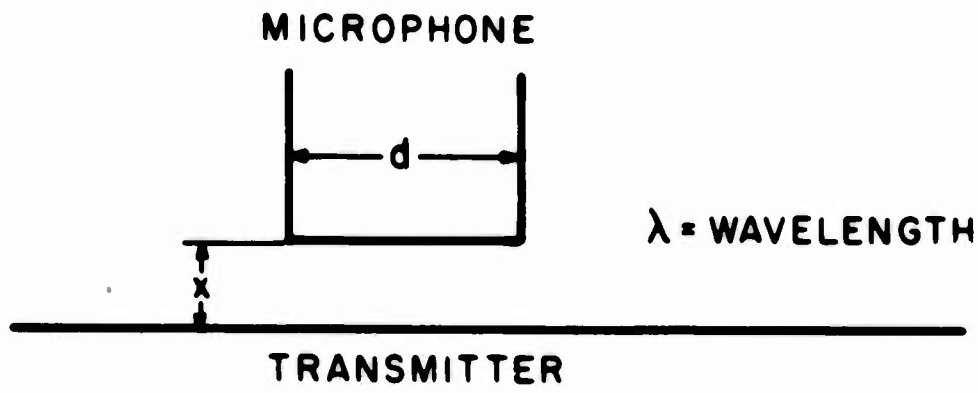

FIG. 12 TRANSMITTER - MICROPHONE SYSTEM

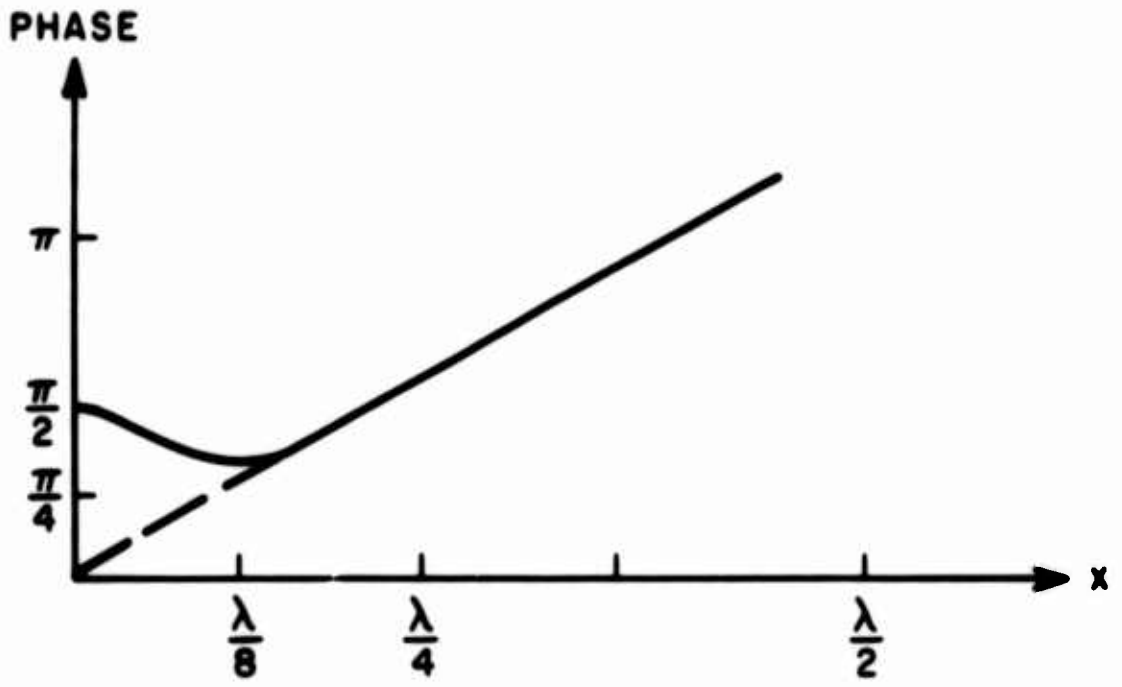

FIG. 13 PHASE AS A FUNCTION OF SEPARATION x

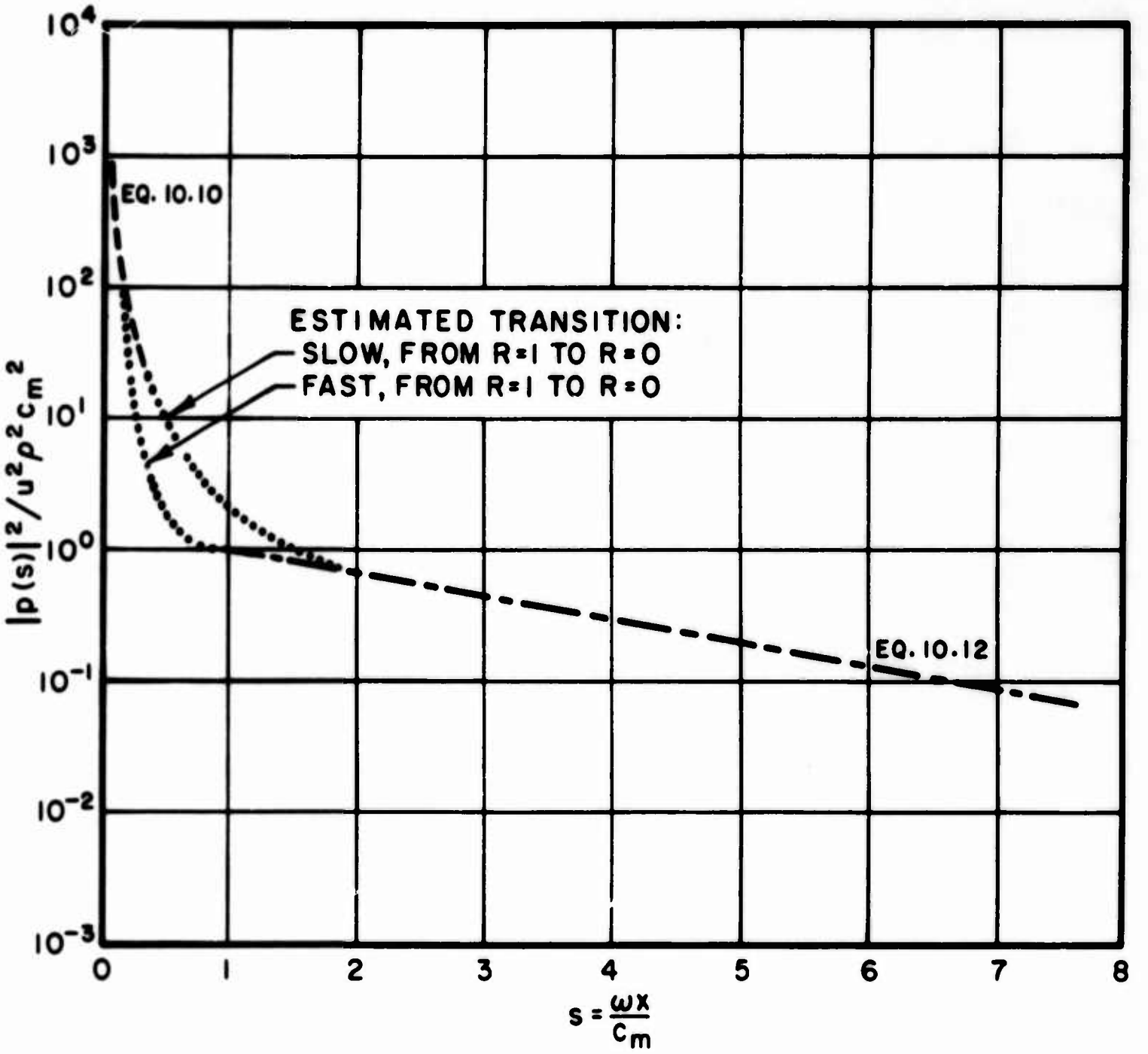

FIG. 14 RELATIVE SOUND PRESSURE LEVEL AS A FUNCTION OF THE NORMALIZED SEPARATION PARAMETER s

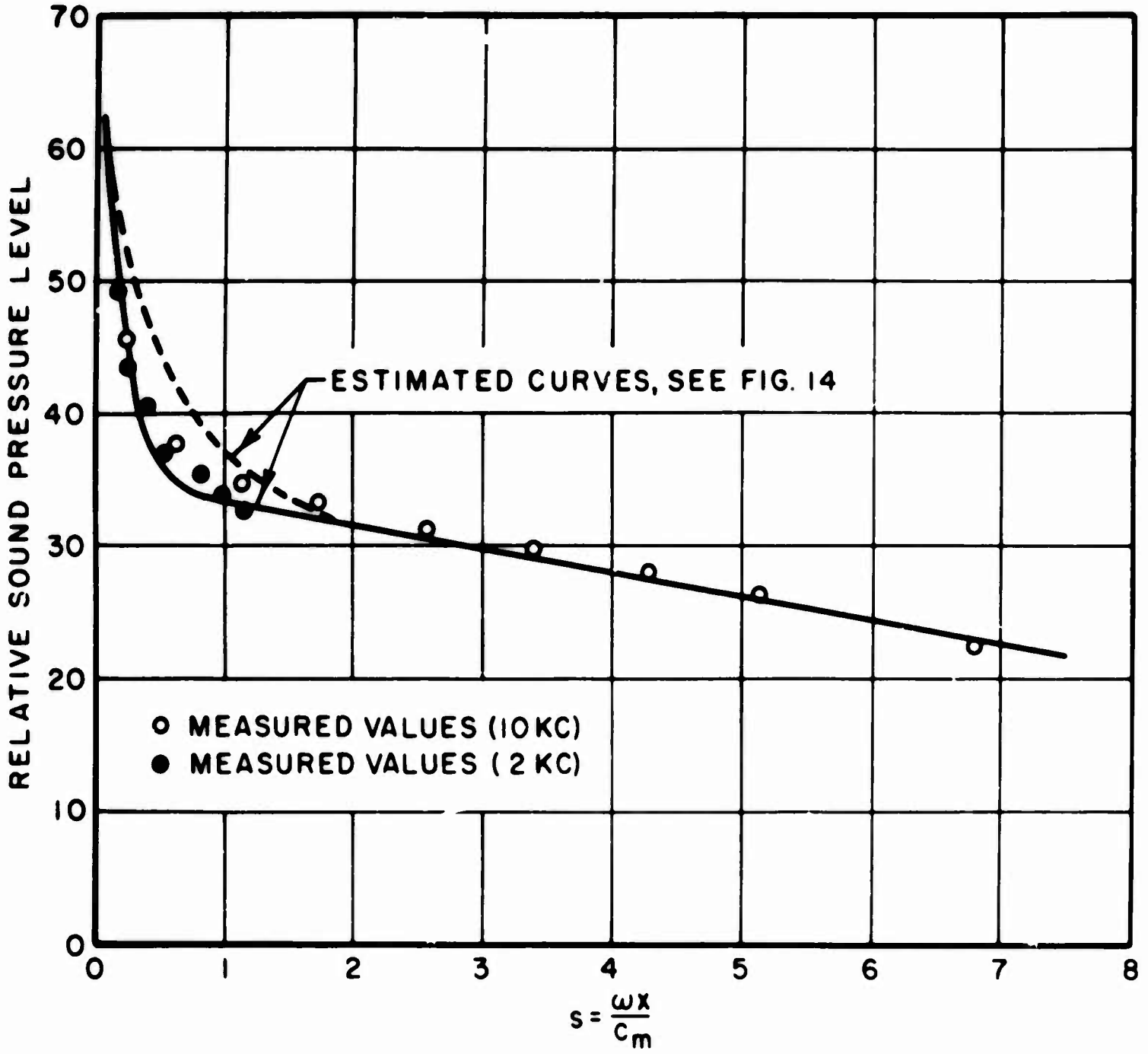

FIG. 15 RELATIVE SOUND PRESSURE LEVEL AS A FUNCTION OF THE NORMALIZED PARAMETER s

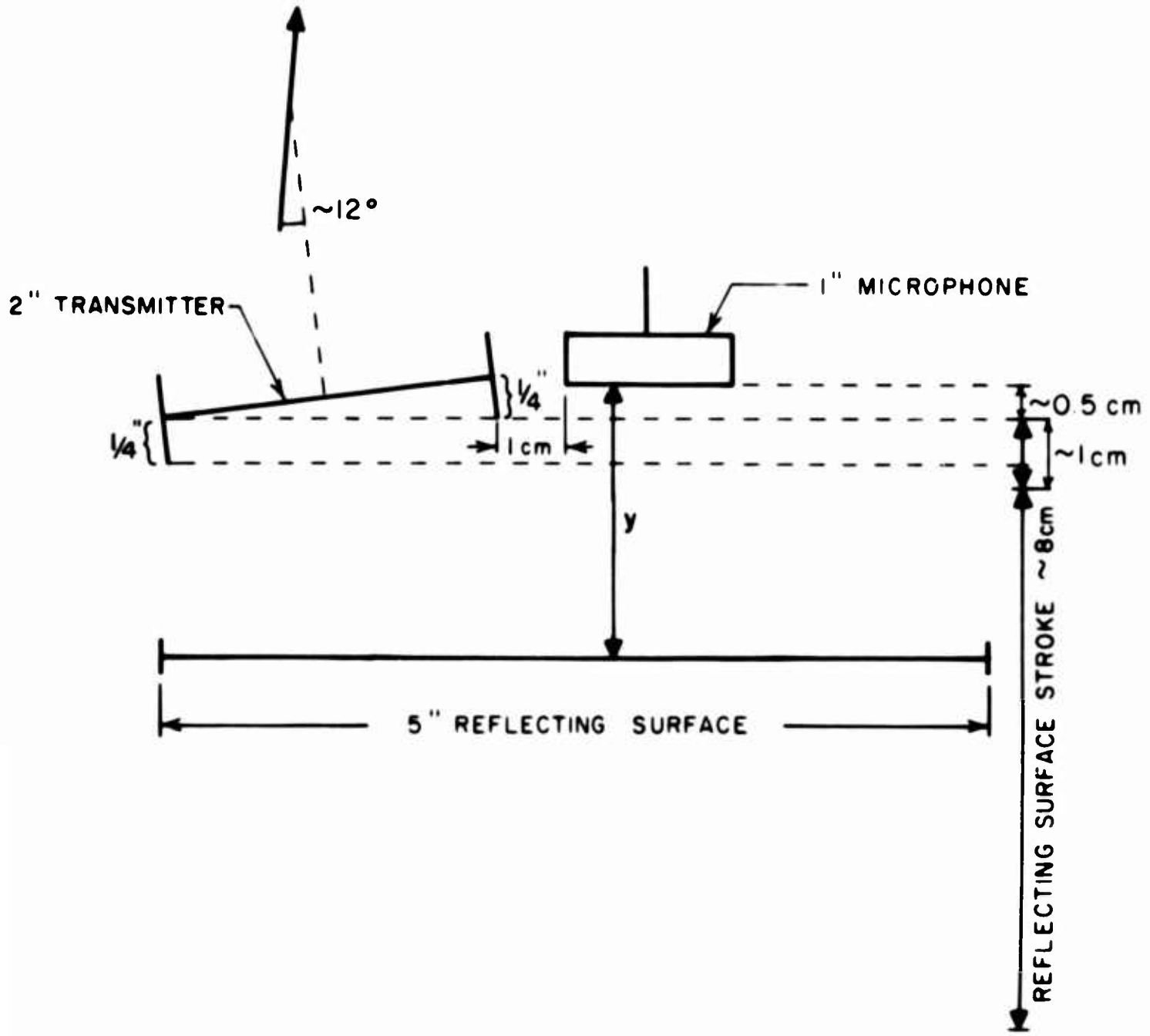

FIG. 16 TRANSMITTER - REFLECTING SURFACE - MICROPHONE SYSTEM

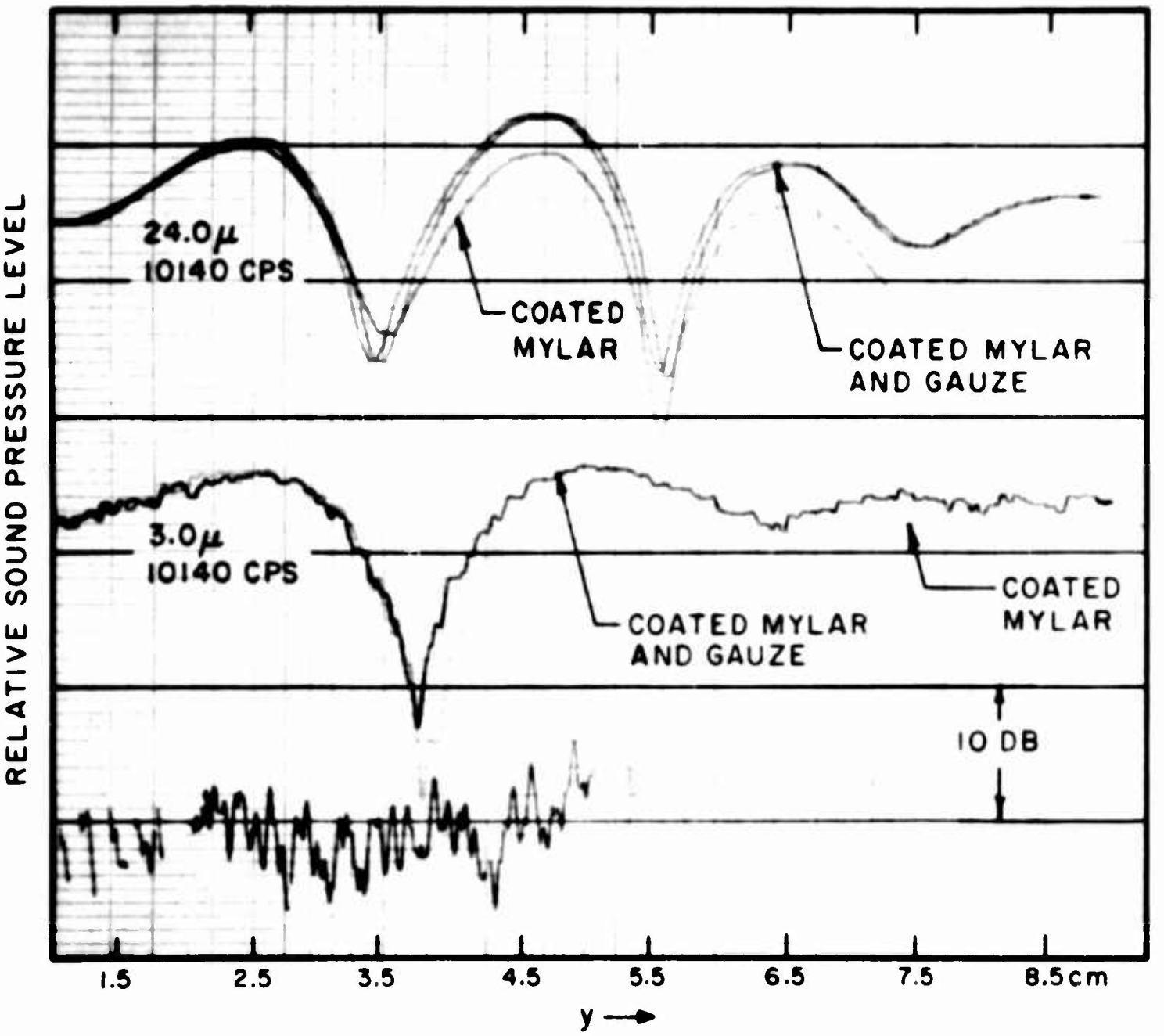

FIG. 17 REFLECTION OF SOUND FROM SURFACES AS A FUNCTION OF SEPARATION

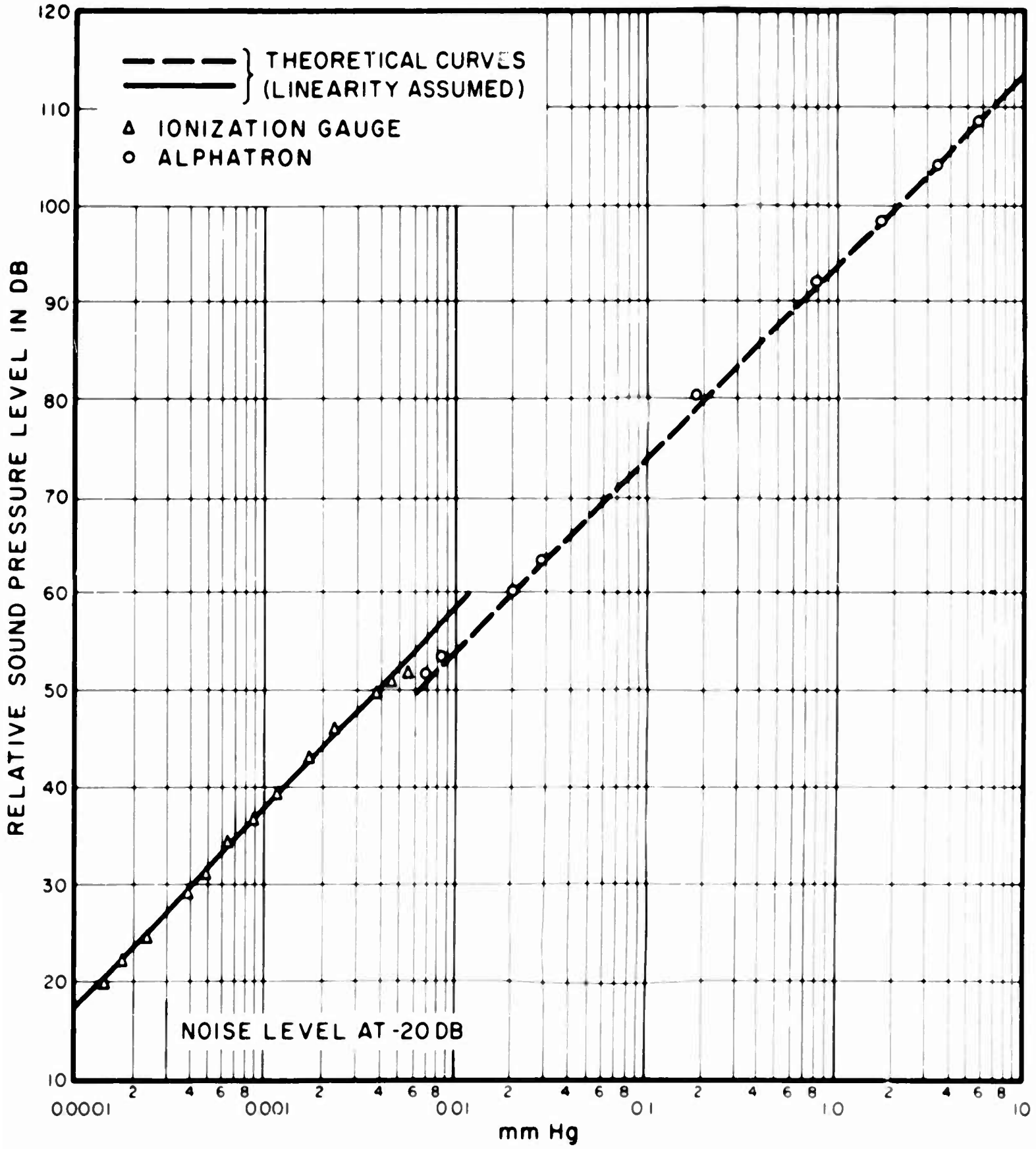

FIG. 18 SOUND PRESSURE LEVEL VS. PRESSURE (FREQUENCY = 6 kc, SEPARATION = 0.35 cm, MICROPHONE DIAMATER = 1 IN., TRANSMITTER DIAMETER = 5.0 IN.)

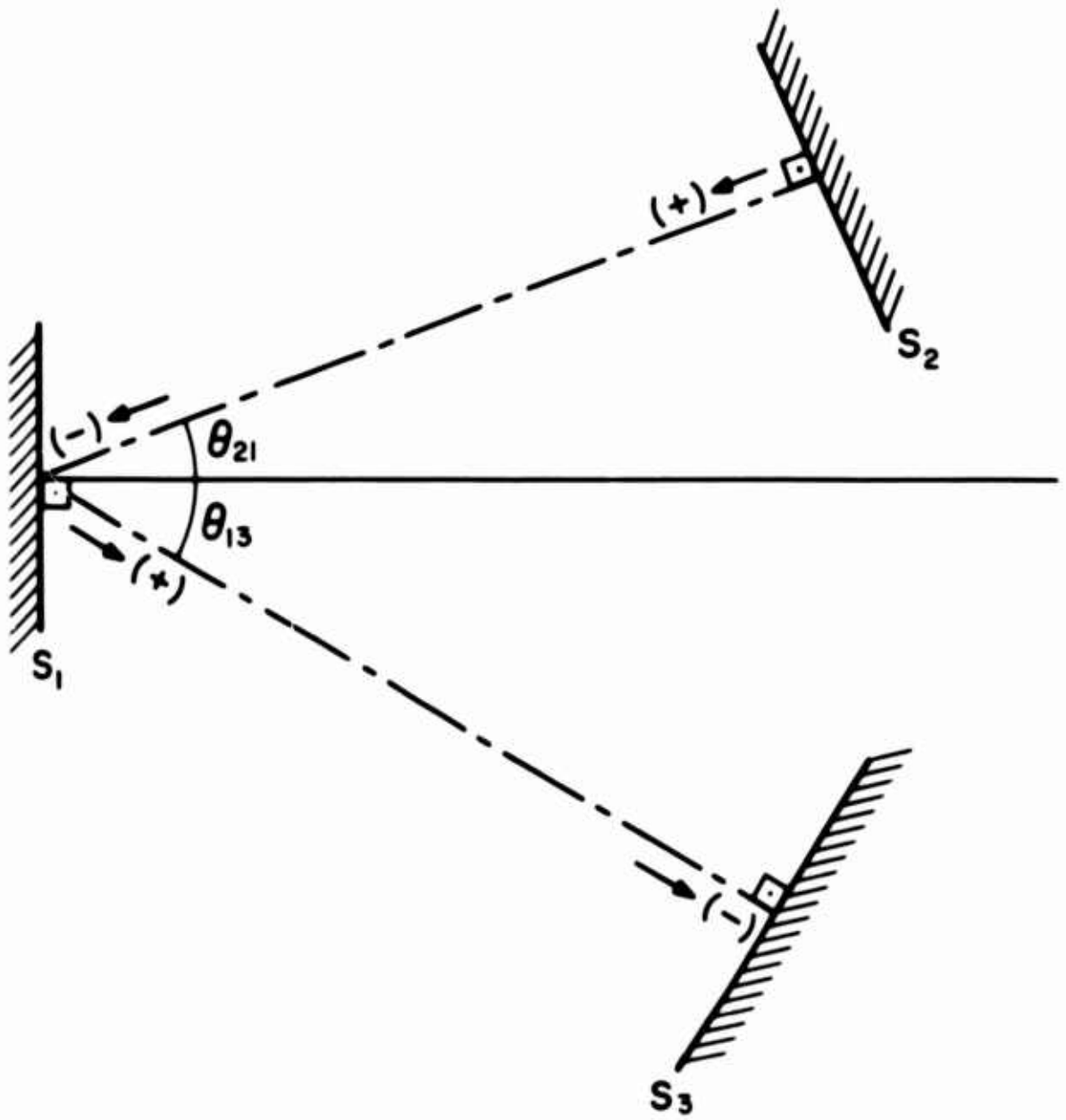

FIG. 19 REFLECTION OF SOUND. S_2 A TRANSMITTER SURFACE, S_1 A REFLECTING SURFACE AND S_3 A RECEIVER SURFACE

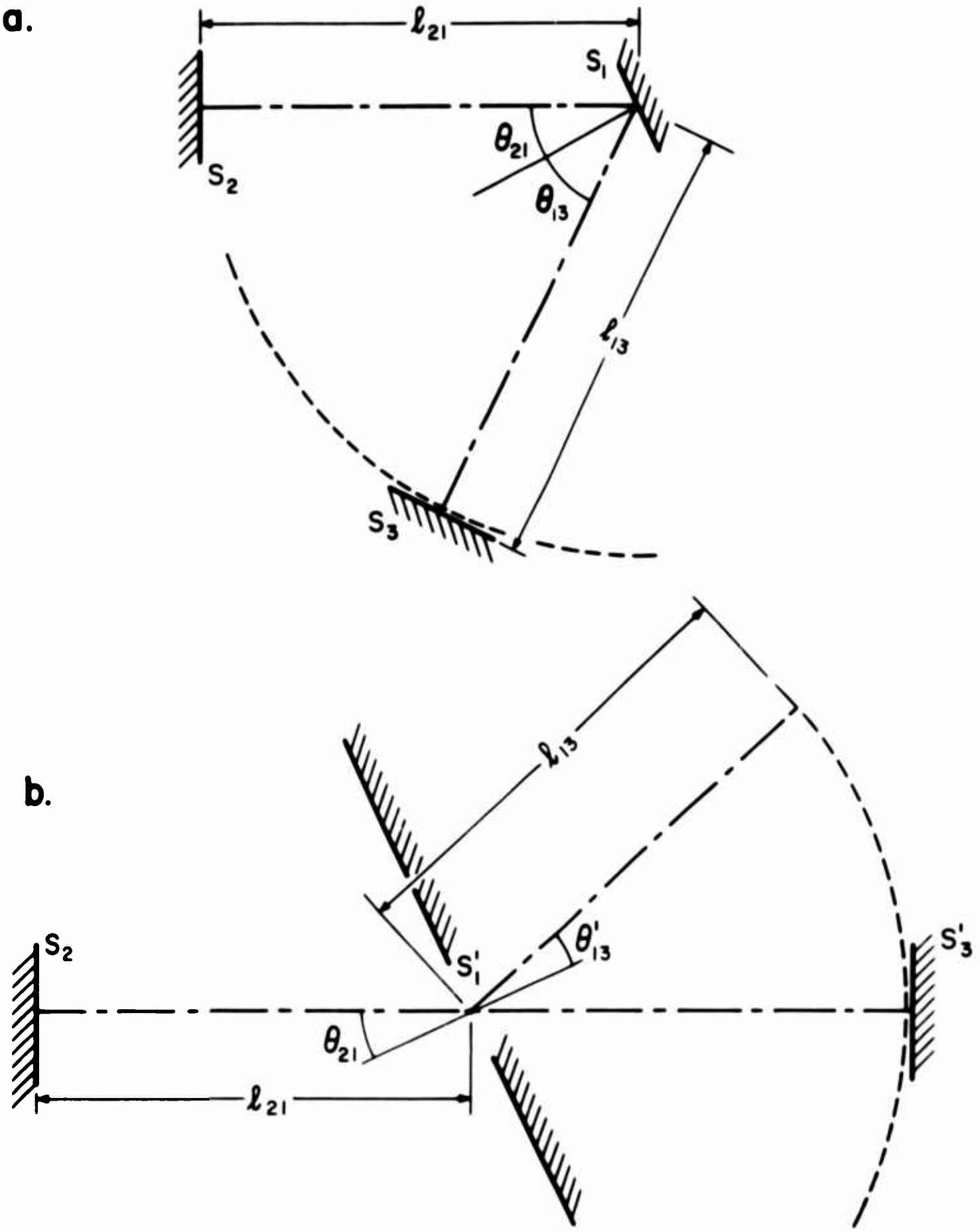

FIG. 20 SCHEMATIC REPRESENTATION OF AN APPARATUS FOR STUDIES OF MOLECULAR-SURFACE INTERACTIONS

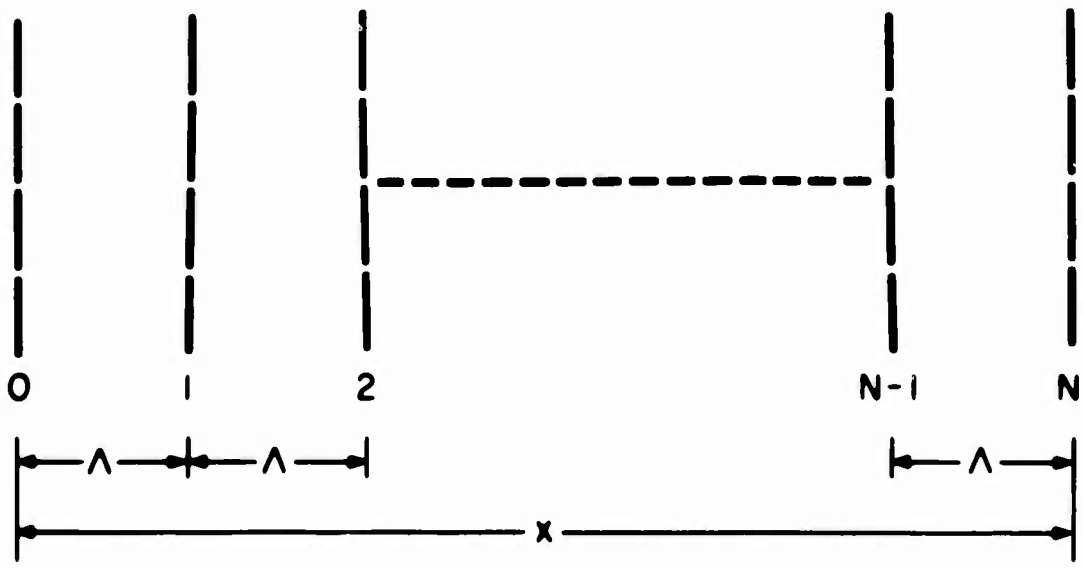

FIG. 21 PROPOSED MODEL FOR KINETIC THEORY OF SOUND PROPAGATION

DISTRIBUTION LIST FOR UNCLASSIFIED
TECHNICAL REPORTS ISSUED UNDER
CONTRACT NONR 3697(00) TASK NR 061-130

Chief of Naval Research
Department of the Navy
Washington 25, D. C.
Attn: Code 438 (3)
419 (1)
421 (1)
461 (1)

Commanding Officer
Office of Naval Research
Branch Office
491 Summer Street
Boston 10, Massachusetts (1)

Commanding Officer
Office of Naval Research
Branch Office
86 East Randolph Street
Chicago 1, Illinois (1)

Commanding Officer
Office of Naval Research
Branch Office
207 West 24th Street
New York 11, New York (1)

Commanding Officer
Office of Naval Research
Branch Office
Navy #100, Box 39
Fleet Post Office
New York, New York (15)

Commanding Officer
Office of Naval Research
Branch Office
1030 East Green Street
Pasadena 1, California (1)

Commanding Officer
Office of Naval Research
Branch Office
1000 Geary Street
San Francisco 9, California (1)

Director
Naval Research Laboratory
Washington 25, D. C.
Attn: Code 2000 (6)
2020 (1)
7411 (Dr. A. C. Kolb) (1)

Commanding Officer and Director
David Taylor Model Basin
Washington 7, D. C.
Attn: Dr. F. N. Frenkiel (Code 108A) (1)
Aerodynamics Laboratory (1)
Library (1)

Chief, Bureau of Naval Weapons
Department of the Navy
Washington 25, D. C.
Attn: Code RMGA-413 (1)
RAAD-34 (1)
RRRE-4 (1)

Commander
U. S. Naval Weapons Laboratory
Dahlgren, Virginia
Attn: Technical Library (1)

Commander
Naval Ordnance Test Station
China Lake, California
Attn: Code 5008 (1)
753 (1)

Commander
Naval Ordnance Laboratory
White Oak, Maryland
Attn: Aeroballistics Division (1)
Aerophysics Division (1)
Ballistics Department (1)
(Dr. A. E. Seigel)
Gas Dynamics Division (1)
Library (1)

Chief, Bureau of Yards and Docks
Department of the Navy
Washington 25, D. C.
Attn: Code 70 (1)
72 (1)

Commanding Officer and Director
U. S. Naval Civil Engineering Lab
Port Hueneme, California
Attn: Code L54 (1)

Superintendent
Naval Postgraduate School
Monterrey, California
Attn: Technical Reports Librarian (1)

Commander
U. S. Naval Missile Center
Point Mugu, California
Attn: Technical Library (1)

Commanding Officer
NROTC & Naval Administrative Unit
Massachusetts Institute of Technology
Cambridge 39, Massachusetts (1)

Commander
Air Force Missile Test Center
AFMTC Technical Library (MU 135)
Patrick Air Force Base, Florida (1)

Executive Director
Air Force Office of Scientific Research
Washington 25, D. C. (1)

Headquarters
DCAS (AFSC)
Attn: DCLMT-TDC
Air Force Unit Post Office
Los Angeles 45, California (1)

J. L. Potter, Manager
Research Branch, VKF
Aro, Incorporated
Arnold Air Force Station
Tennessee (2)

Mr. Lukasiewicz, Chief
Gas Dynamics Facility
Aro, Incorporated
Arnold Air Force Station
Tennessee (1)

HQ AFLC (MCEEE)
Wright-Patterson Air Force Base
Ohio (1)

Commander
Wright-Air Development Command
Wright-Patterson Air Force Base
Ohio
Attn: Library (1)

ASD (ASRMDF-1)
Wright-Patterson Air Force Base
Ohio (1)

ARL (ARN)
Building 450
Wright-Patterson Air Force Base
Ohio (1)

Elmer G. Johnson, Chief
Fluid Dynamics Facilities Branch
Aeronautical Research Laboratory
Wright-Patterson Air Force Base, Ohio (1)

United States Army Research Office
(Durham)
Box CM, Duke Station
Durham, North Carolina (1)

Commanding General
Aberdeen Proving Ground, Maryland
Attn: Technical Library (EBL) (1)

Dr. J. H. Frazer
Internal Ballistics Laboratory
Aberdeen Proving Ground, Maryland (1)

Dr. C. W. Lampson
Technical Director
Ballistic Research Laboratories
Aberdeen Proving Ground, Maryland (1)

Chief
Defense Atomic Support Agency
Washington 25, D. C. (1)

Dr. J. Sternberg
Ballistics Research Laboratory
Aberdeen Proving Ground, Maryland (1)

Dr. F. D. Bennett
Exterior Ballistics Laboratory
BRL
Aberdeen Proving Ground, Maryland (1)

Executive Secretary
Weapons System Evaluation Group
Office of the Secretary of Defense
The Pentagon
Washington 25, D. C. (1)

Ames Research Center
National Aeronautics and Space
Administration
Moffett Field, California
Attn: Library (1)

Langley Research Center
National Aeronautics and Space Administration
Langley Station
Hampton, Virginia
Attn: Library (1)

Lewis Research Center
National Aeronautics and Space Administration
21000 Brookpark Road
Cleveland 35, Ohio
Attn: Library (1)

National Aeronautics and Space Administration
150 Pico Boulevard
Santa Monica, California (1)

Director
National Bureau of Standards
Washington 25, D. C.
Attn: Electron Physics Section (1)
Equation of State Section (1)
Fluid Mechanics Section (1)
Mathematical Physics Section (1)
Library (1)
Dr. D. H. Tsai (1)

Dr. R. N. Thomas
National Bureau of Standards
Boulder Laboratories
Boulder, Colorado (1)

U. S. Atomic Energy Commission
Office of Technical Information Extension
P. O. Box 62

U. S. Atomic Energy Commission
Technical Information Service
Washington 25, D. C.
Attn: Technical Librarian (1)

National Science Foundation
Division of Mathematical, Physical, and Engineering Sciences
Washington 25, D. C.
Attn: Engineering Sciences Program Office (1)

Armed Services Technical Information Agency
Arlington Hall Station
Arlington 12, Virginia (10)

Dr. M. Abele
General Applied Science Lab, Inc.
Westbury, Long Island, New York (1)

Professor J. D. Akerman
Institute of Technology
University of Minnesota
Minneapolis 14, Minnesota (1)

Professor W. Bleakney
Palmer Physical Laboratory
Princeton University
Princeton, New Jersey (1)

Dr. Jack N. Nielsen
Vidya, Incorporated
2626 Hanover Street
Palo Alto, California (1)

Professor G. L. Von Eschen
Department of Aeronautical and Astronautical Engineering
Ohio State University
2036 Neil Avenue
Columbus 10, Ohio (1)

Professor Antonio Ferri
Aerodynamics Laboratory
Polytechnic Institute of Brooklyn
527 Atlantic Avenue
Freeport, New York (1)

Professor R. G. Fowler
Physics Department
University of Oklahoma
Norman, Oklahoma (1)

Dr. I. I. Glass
Institute of Aerophysics
University of Toronto
Toronto 5, Ontario, Canada (1)

Professor D. F. Hornig, Chairman
Chemistry Department
Princeton University
Princeton, New Jersey (1)

Dr. Arthur Kantorwitz, Director
AVCO-Everett Research Laboratory
2385 Revere Beach Parkway
Everett 49, Massachusetts (1)

Professor Otto Laporte
University of Michigan
Physics Department
Ann Arbor, Michigan (1)

Professor H. Liepmann
Department of Aeronautics
California Institute of Technology
Pasadena 4, California (1)

Professor G. S. S. Ludford
Department of Mechanics
Cornell University
Ithaca, New York (1)

Dr. F. K. Moore, Director
Aero-Sciences Division
Cornell Aeronautical Laboratory, Inc.
P. O. Box 235
Buffalo 21, New York (1)

Dr. Boris Ragent
Vidya, Incorporated
2626 Hanover Street
Palo Alto, California (1)

Professor E. L. Resler
Graduate School of Aeronautical
Engineering
Cornell University
Ithaca, New York (1)

Dr. S. A. Schaaf
University of California
Department of Engineering
Berkeley, California (1)

Professor A. H. Shapiro
Department of Mechanical Engineering
Massachusetts Institute of Technology
Cambridge 39, Massachusetts (1)

Professor P. Sherman
Aeronautical Engineering Department
University of Michigan
Ann Arbor, Michigan (1)

Professor K. Stewartson
Department of Mathematics
University of Durham
Science Laboratories
South Road
Durham, England (1)

Professor O. H. Theimer
Research Professor
New Mexico State University
Research Center, Box 756
University Park, New Mexico (1)

Professor A. B. Arons
Department of Physics
Amherst University
Amherst, Massachusetts (1)

Division of Applied Mathematics
Brown University
Providence 12, Rhode Island (1)

Professor Kestin
Division of Engineering
Brown University
Providence 12, Rhode Island (1)

Professor Maeder
Division of Engineering
Brown University
Providence 12, Rhode Island (1)

Engineering Division
California Institute of Technology
Pasadena 4, California (1)

Jet Propulsion Laboratory
4800 Oak Grove Dirve
Pasadena, California
Attn: Library (1)

Professor M. S. Plesset
Engineering Division
California Institute of Technology
Pasadena 4, California (1)

Professor C. B. Millikan, Director
Guggenheim Aeronautical Laboratory
California Institute of Technology
Pasadena 4, California (1)

Professor L. Lees
Guggenheim Aeronautical Laboratory
California Institute of Technology
Pasadena 4, California (1)

(1) Professor F. Zwicky
Department of Physics
California Institute of Technology
Pasadena 4, California (1)

Professor G. Kuerti
1) Department of Mechanical Engineering
Case Institute of Technology
10900 Euclid Avenue
Cleveland 6, Ohio (1)

1) Professor P. Kusch
Columbia University
New York, New York (1)

1) Professor W. Sears
Graduate School of Aeronautical
Engineering
Cornell University
Ithaca, New York (1)

1) Dr. A. Hertzberg
Cornell Aeronautical Laboratory
4455 Genesse Street
Buffalo, New York (1)

1) Dr. Miller
Denver Research Institute
University Park Campus
) Denver University
Denver 10, Colorado (1)

Professor G. F. Carrier
Pierce Hall
) Harvard University
Cambridge 38, Massachusetts (1)

Professor H. Emmons
Department of Engineering Sciences
) Harvard University
Cambridge 38, Massachusetts (1)

Professor L. Goldberg
Harvard College Observatory
) Cambridge 38, Massachusetts (1)

Dr. Fred L. Whipple
60 Garden Street
Cambridge 38, Massachusetts (1)

Armour Research Foundation
10 West 35th Street
Chicago 16, Illinois (1)

School for Applied Mathematics
Indiana University
Bloomington, Indiana (1)

Professor F. H. Clauser
Department of Aeronautics
Johns Hopkins University
Baltimore 18, Maryland (1)

Professor R. J. Emrich
Department of Physics
Lehigh University
Bethlehem, Pennsylvania (1)

Professor I, Amdur
Massachusetts Institute of Technology
Cambridge, Massachusetts (1)

Professor George A. Brown
Massachusetts Institute of Technology
3-164
77 Massachusetts Avenue
Cambridge 39, Massachusetts (1)

Professor H. C. Hottel
Department of Chemical Engineering
Massachusetts Institute of Technology
Cambridge 39, Massachusetts (1)

Dr. L. Trilling
Department of Aeronautics and
Astronautics
Massachusetts Institute of Technology
Cambridge 39, Massachusetts (1)

Dr. Lee Arnold
College of Engineering
New York University
University Heights
New York 53, New York (1)

AF Cambridge Research Lab
L. G. Hanscom Field
Bedford, Massachusetts
Attn: Polly Condon,
Technical Library (1)

Professor C. C. Lin
Department of Mathematics
Massachusetts Institute of Technology
Cambridge 39, Massachusetts (1)

Department of Mechanical Engineering
Massachusetts Institute of Technology
Cambridge 39, Massachusetts (1)

Professor B. Bederson
Physics Department
New York University
University Heights
New York 53, New York (1)

Professor J. J. Stoker
Institute of Mathematical Sciences
4 Washington Place
New York 3, New York (1)

Professor J. F. Ludloff
Guggenheim School of Aeronautics
New York University
New York 53, New York (1)

Professor Ali Bulent Cambel
Department of Mechanical Engineering
Northwestern University
Evanston, Illinois (1)

Dr. Loren E. Bollinger
The Ohio State University
Rocket Research Laboratory
2240 Olentangy River Road
Columbus 10, Ohio (1)

Professor R. G. Stoner
Department of Physics (Osmond)
Pennsylvania State University
University Park, Pennsylvania (1)

Professor W. D. Hayes
Forrestal Research Center
Princeton, New Jersey (1)

Professor S. Bodgonoff
Department of Aeronautical Engineering
Princeton University
Princeton, New Jersey (1)

Professor L. Spitzer, Jr.
Princeton University Observatory
Princeton, New Jersey (1)

Professor J. Foa
Department of Aeronautical Engineering
Rensselaer Polytechnic Institute
Troy, New York (1)

Dr. C. Cook
Stanford Research Institute
Menlo Park, California (1)

Professor D. Gilbarg
Applied Mathematics and Statistics
Laboratory
Stanford University
Stanford, California (1)

Professor Milton van Dyke
Department of Aeronautical Engineering
Stanford University
Stanford, California (1)

Professor D. Bershader
Department of Aeronautical Engineering
Stanford University
Stanford, California (1)

Professor Allen Chapmann, Chairman
Mechanical Engineering Department
William M. Rice Institute
Box 1892
Houston 1, Texas (1)

Professor M. Holt
Division of Aeronautical Sciences
University of California
Berkeley 4, California (1)

Professor W. A. Nierenberg
University of California
Berkeley, California (1)

Professor A. K. Oppenheim
Division of Mechanical Engineering
University of California
Berkeley 4, California (1)

Dr. S. A. Colgate
Radiation Laboratory
University of California
Livermore, California (1)

Dr. R. Post
Radiation Laboratory
University of California
Livermore, California (1)

Dr. Duff
Los Alamos Scientific Laboratory
University of California
Los Alamos, New Mexico (1)

Dr. J. L. Tuck
Physics Division
Los Alamos Scientific Laboratory
University of California
Los Alamos, New Mexico (1)

Dr. R. G. Shreffler
4114 Washington Street
Midland, Michigan (1)

Professor A. F. Charwat
Department of Engineering
University of California
Los Angeles 24, California (1)

Dean L. M. K. Boelter
College of Engineering
U. C. L. A.
Los Angeles, California (1)

Director
Engineering Center
University of Southern California
University Park
Los Angeles 7, California (1)

Professor J. Kaplan
Department of Physics
U.C.L.A.
Los Angeles, California (1)

Aeronautical Sciences Laboratory
University of California
Richmond Field Station
1301 South 46th Street
Richmond, California (1)

Professor R. Donnelly
Institute for the Study of Metals
University of Chicago
5640 Ellis Avenue
Chicago 37, Illinois (1)

Professor R. P. Harringotn, Head
Department of Aeronautical Engineering
University of Cincinnati
Cincinnati 21, Ohio (1)

Professor T. L. Bailey
Department of Physics
University of Florida
Gainesville, Florida (1)

Dr. H. Kendall Reynolds
Physics Department
University of Houston
3801 Cullen Boulevard (1)

Professor A. H. Taub
114 Digital Computer Laboratory
University of Illinois
Urbana, Illinois (1)

Professor H. S. Stillwell, Chairman
Department of Aeronautical and
Astronautical Engineering
University of Illinois
Urbana, Illinois (1)

Professor H. R. Griem
University of Maryland
College Park, Maryland (1)

Professor Pai
Institute for Fluid Mechanics and
Applied Mathematics
University of Maryland
College Park, Maryland (1)

Professor Burgers
Institute for Fluid Mechanics and
Applied Mathematics
University of Maryland
College Park, Maryland (1)

Professor G. E. Uhlenbeck
The Rockefeller Institute
New York 21, New York (1)

Professor A. Kuethe
Department of Aeronautical Engineering
University of Michigan
Ann Arbor, Michigan (1)

Professor W. C. Nelson
Department of Aeronautical Engineering
University of Michigan
Ann Arbor, Michigan (1)

Professor Keeve M. Siegel
Radiation Laboratory
The University of Michigan
201 Catherine Street
Ann Arbor, Michigan (1)

Dr. M. A. Biondi
Physics Department
University of Pittsburgh
Pittsburgh, Pennsylvania (1)

Professor T. M. Donahue
University of Pittsburgh
Pittsburgh Pennsylvania (1)

M. J. Thompson
Defense Research Laboratory
University of Texas
P. O. Box 8029
Austin, Texas (1)

The Library
Institute of Aerophysics
University of Toronto
Toronto 5, Ontario (1)

Professor M. A. Cook, Director
Experimental Research Group
University of Utah
Salt Lake City, Utah (1)

A. R. Kuhlthau, Director
Research Laboratories for the
Engineering Sciences
Thronton Hall
University of Virginia
Charlottesville, Virginia (1)

Department Librarian
Department of Aeronautical Engineering
University of Washington
Seattle 5, Washington (1)

Professor J. O. Hirschfelder
Theoretical Chemistry Laboratory
University of Wisconsin
Post Office Box 2127
Madison 5, Wisconsin (1)

Aerojet-General Corporation
Attn: Myra T. Grenier, Librarian
6352 N. Irwindale Avenue
Azusa, California (1)

William H. Dorrance, Head
Aero-Analysis Department
2400 East El Segundo Boulevard
El Segundo, California (1)

American Machine and Foundry Company
Attn: Mechanics Research Department
7501 N. Natchez Avenue
Niles, Illinois (1)

Australian Weapons Research
Establishment
c/o Defense Research and Development
Australian Joint Service Staff
P. O. Box 4837
Washington 8, D. C. (1)

Dr. S. C. Lin
Avco-Everett Research Laboratory
2385 Revere Beach Parkway
Everett 49, Massachusetts (1)

Mr. W. T. Hamilton (M.S. 15-34)
Chief of Flight Technology
The Boeing Company
Aero-Space Division
P. O. Box 3707
Seattle 24, Washington (1)

Technical Information Center
Chance Vought Corporation
P. O. Box 5907
Dallas 22, Texas (1)

Dr. A. E. S. Green
Chief of Physics
General Dynamics-Convair
Mail Zone 6-172
San Diego 12, California (1)

N. A. Baird, G-25
Douglas Aircraft Company, Inc.
3000 Ocean Park Boulevard
Santa Moncia, California (1)

Fairchild Engine and Aircraft Company
Guided Missiles Division
Wyabdanch, Long Island, New York (1)
(1)

Dr. J. S. Isenberg
Technical Director
Flight Sciences Laboratory, Inc.
1965 Sheridan Drive
(1) Buffalo 23, New York (1)

Dr. W. Fite
General Atomic
P. O. Box 608
) San Diego 12, California (1)

Mr. Lawrence I. Chasen, Manager
MSVD Library
General Electric Company
Missile and Space Vehicle Department
1) 3198 Chestnut Street
Philadelphia 1, Pennsylvania (1)

Dr. Nagamatsu
General Electric Company
1) Research Laboratory
P. O. 1088
Schenectady, New York (1)

Dr. Doanald R. White
General Electric Company
Research Laboratory
) P. O. Box 1088
Schenectady, New York (1)

Dr. Alpher
General Electric Company
) Research Laboratory
P. O. Box 1088
Schenectady, New York (1)

Dr. G. Wehner
General Mills, Inc.
) Electronics Group
2003 E. Hennepin Avenue
Minneapolis 13, Minnesota (1)

Dr. Robert N. Hollyer, Jr.
) Research Laboratories
General Motors Corporation
12 Mile and Mound Road
Warren, Michigan (1)

Engineering Library
Grumman Aircraft Engineering Corp.
Bethpage, Long Island, New York (1)

Mr. E. O. Marriott
Hughes Aircraft Company
Building 6/Mail Station A1066
Culver City, California (1)

Mr. Marshall P. Tulin
Hydronautics, Inc.
200 Monroe Street
Rockville, Maryland (1)

Dr. H. Cohen
IBM Research Center
P. O. Box 218
Yorktown Heights, New York (1)

Mr. Ronald Smelt
Chief Scientist
Lockheed Missiles and Space Company
P. O. Box 504
Sunnyvale, California (1)

Dr. L. Ridenour
Lockheed Aircraft Missile
Systems Division
Van Nuys, California (1)

Engineering Library
The Marquardt Corporation
16555 Saticoy
Van Nuys, California (1)

Mr. L. G. Cooper
The Martin Company
Department 2550, Mail No. J-3072
Baltimore 3, Maryland (1)

The Martin Company
DATAC, Research Library, A-52
P. O. Box 179
Denver 1, Colorado (1)

Dr. S. L. Levy, Director
Midwest Research Institute
Physics and Mathematics Division
425 Volker Boulevard
Kansas City 10, Missouri (1)

Midwest Research Institute
Attn: Library
425 Volker Boulevard
Kansas City 10, Missouri (1)

Dr. N. C. Freeman
National Physical Laboratory
Teddington, Middlesex, England (1)

Mr. K. Orlik-Ruckermann
Head, Unsteady Aerodynamics
National Aeronautical Establishment
National Research Council
Ottawa 2, Canada (1)

Dr. E. R. van Driest
North American Aviation, Inc.
Space and Information Systems Division
12214 Lakewood Boulevard
Downey, California (1)

Northrop Corporation
Norair Division
Attn: Technical Information
1001 E. Broadway
Hawthorne, California (1)

Ramo Wooldridge Corporation
A Division of Thompson Ramo Wooldridge
Incorporated
Attn: Technical Information Services
8433 Fall Brook Avenue
Canoga Park, California (1)

Mr. E. Williams
Rand Corporation
1700 Main Street
Santa Monica, California (1)

Dr. R. W. Perry, Chief
Re-Entry Simulation Laboratory
Applied Research & Development
Republic Aviation Corporation
Farmingdale, New York (1)

Republic Aviation Corporation
Attn: Mr. E. A. Simkovich
Space Systems and Research
Farmingdale, Long Island, New York (1)

Dr. L. F. Crabtree
Ministry of Aviation
Royal Aircraft Establishment
Aerodynamics Department
Farnborough, Hants, England (1)

Dr. J. D. Shreve, Jr. 5112
Sandia Corporation
Sandia Base
Albuquerque, New Mexico (1)

Mr. C. C. Hudson
Sandia Corporation
Sandia Base
Albuquerque, New Mexico (1)

Mr. R. S. Claassen, Director
Physical Research
Sandia Corporation
Sandia Base
Albuquerque, New Mexico (1)

Dr. H. G. Lew
Manager, Gas Dynamics
Space Sciences Laboratory
Space Technology Center
King of Prussia, Pennsylvania (1)

Dr. A. Ritter
Therm Advanced Research
Therm, Incorporated
Ithaca, New York (1)

United Aircraft Corporation
Research Laboratories
400 Main Street
East Hartford 8, Connecticut (1)

Dr. Donald E. Davenport, Director
Poulter Laboratories
Stanford Research Institute
Menlo Park, California (1)

Dr. Duvall
Stanford Research Institute
Poulter Laboratories
Menlo Park, California (1)

Scientific and Technical Information
Facility
Attn: NASA Representative
P. O. Box 5700
Bethesda, Maryland (1)

Professor Walter Vali
Department of Aeronautical Engineering
Stanford University
Stanford, California (1)

Dr. Manfred M. Hecal
Müller-BBM GmbH
Der Hospitalstrasse 10
München 2
Germany (1)

Mithras, Incorporated
380 Putnam Avenue
Cambridge 39, Massachusetts
Attn: Dr. E. S. Rubin (1)

AVCO Research and Advanced
Development Division
201 Lowell Street
Wilmington, Massachusetts
Attn Chief of Aerodynamics (1)

Professor P. Courant
Institute of Mathematical Sciences
New York University
25 Waverly Place
New York 3, New York (1)

Dr. J. Menkes
Institute for Defense Analyses
1666 Connecticut Avenue, N. W.
Washington 9, D. C. (1)

Professor J. H. Clarke
Division of Engineering
Brown University
Providence 12, Rhode Island (1)

Professor Walter G. Vincenti
Department of Aeronautics and
Astronautics
Stanford University
Stanford, California (1)

Dr. W. J. Christian
Armour Research Foundation
Illinois Institute of Technology
10 West 35th Street
Chicago 16, Illinois (1)

Professor R. Vaglio-Laurin
Aerodynamics Laboratory
Polytechnic Institute of Brooklyn
527 Atlantic Avenue
Freeport, New (1)

Stanford Research Institute
333 Ravenswood Avenue
Menlo Park, California
Attn: Myles R. Berg (1)

Professor G. N. Patterson
University of Toronto
Institute of Aerophysics
Toronto 5, Canada (1)

Professor Ting Li
Department of Aerospace Engineering
University of Cincinnati
Cincinnati 21, Ohio (1)

Professor D. Mintzer
Department of Mechanical Engineering
Northwestern University
Technological Institute
Evanston, Illinois (1)

Professor P. P. Wegener
Department of Engineering and Applied
Sciences
Yale University
New Haven, Connecticut (1)

Professor R. F. Probstein
Department of Mechanical Engineering
Massachusetts Institute of Technology
Cambridge 39, Massachusetts (1)

A. Reifman
Astrophysics Research Corporation
2444 Wilshire Boulevard
Santa Monica, California (1)

Army Missile Command
Redstone Arsenal, Alabama
Attn: Mr. W. Lindberg (1)
Technical Library (1)

E. Haynes
Advanced Research Projects Agency
The Pentagon
Washington 25, D. C. (1)
Attn: Dr. C. McLain (1)

AF Rome Air Development Center
Griffiss Air Force Base
Rome, New York
Attn: Documents Library RCOIL-2 (1)

Aerospace Corporation
P. O. Box 95085
Los Angeles 45, California
Attn: W. J. Bennison, Librarian (1)

AVCO-Everett Research Laboratory
2385 Revere Beach Parkway
Everett 49, Massachusetts
Attn: Barbara Spence, Technical Library (1)

AVCO Corporation
201 Lowell Street
Wilmington, Massachusetts
Attn: Theodore Rupprecht, Chief
Research Library (1)

Battelle Memorial Institute
505 King Avenue
Columbus 1, Ohio
Attn: BMI-DEFENDER, Margaret Ann Long (3)

Bell Telephone Laboratories, Inc.
Whippany Laboratory
Whippany, New Jersey
Attn: Lloyd F. Wagner
Classified Library, 2A-1658 (1)

General Dynamics Corporation
Astronautics Division
Box 1128
San Diego 12, California
Attn: Engineering Library (1)

General Motors Corporation
Defense Systems Division
Box T
Santa Barbara, California
Attn: Gail T. Flesher (1)

Heliodyne Corporation
117 East Colorado Boulevard
Pasadena, California
Attn: Dr. Saul Feldman (1)

Massachusetts Institute of Technology
Lincoln Laboratory
P. O. Box 73
Lexington 73, Massachusetts
Attn: Mary A. Granese, Librarian (1)
Seymour Edelberg (1)
Dr. Glen F. Pippert (1)

Radio Corporation of America
Missile and Surface Radar Division
Moorestown, New Jersey
Attn: Gertrude Pushner
Eng. Library 127-223 (1)

Office of Technical Services
Department of Commerce
Washington 25, D. C. (1